



FLASHMOTION: FEW-STEP CONTROLLABLE VIDEO GENERATION WITH TRAJECTORY GUIDANCE

Quanhao Li^{1,2} Zhen Xing^{1,2} Rui Wang^{1,2} Haidong Cao^{1,2}
Qi Dai³ Daoguo Dong^{1,2} Zuxuan Wu^{1,2,†}

¹Institute of Trustworthy Embodied AI, Fudan University,

²Shanghai Key Laboratory of Multimodal Embodied AI, ³Microsoft Research Asia

Abstract

Recent advances in trajectory-controllable video generation have achieved remarkable progress. Previous methods mainly use adapter-based architectures for precise motion control along predefined trajectories. However, all these methods rely on a multi-step denoising process, leading to substantial time redundancy and computational overhead. While existing video distillation methods successfully distill multi-step generators into few-step, directly applying these approaches to trajectory-controllable video generation results in noticeable degradation in both video quality and trajectory accuracy. To bridge this gap, we introduce **FlashMotion**, a novel training framework designed for few-step trajectory-controllable video generation. We first train a trajectory adapter on a multi-step video generator for precise trajectory control. Then, we distill the generator into a few-step version to accelerate video generation. Finally, we finetune the adapter using a hybrid strategy that combines diffusion and adversarial objectives, aligning it with the few-step generator to produce high-quality, trajectory-accurate videos. For evaluation, we introduce **FlashBench**, a benchmark for long-sequence trajectory-controllable video generation that measures both video quality and trajectory accuracy across varying numbers of foreground objects. Experiments on two adapter architectures show that FlashMotion surpasses existing video distillation methods and previous multi-step models in both visual quality and trajectory consistency.

Code: <https://github.com/quanhaol/FlashMotion>

Website: <https://quanhaol.github.io/flashmotion-site/>

1 Introduction

The emergence of diffusion models [12, 35, 36] has significantly advanced the field of video generation, enabling recent models [8, 16, 40, 50, 52, 53, 55, 64] to synthesize high-quality videos directly from textual or visual inputs. Building on these advances, trajectory-controllable video generation further introduces user-defined motion control, allowing videos to be generated following specified trajectory patterns [5, 18, 26, 41, 57, 62, 63]. Despite their impressive generative capability, previous methods require multiple denoising steps, and directly using fewer steps can lead to severe blurry artifacts as shown in Fig. 1 (a).

To address this high computational burden, recent video distillation methods have been proposed to distill

[†]Corresponding authors.

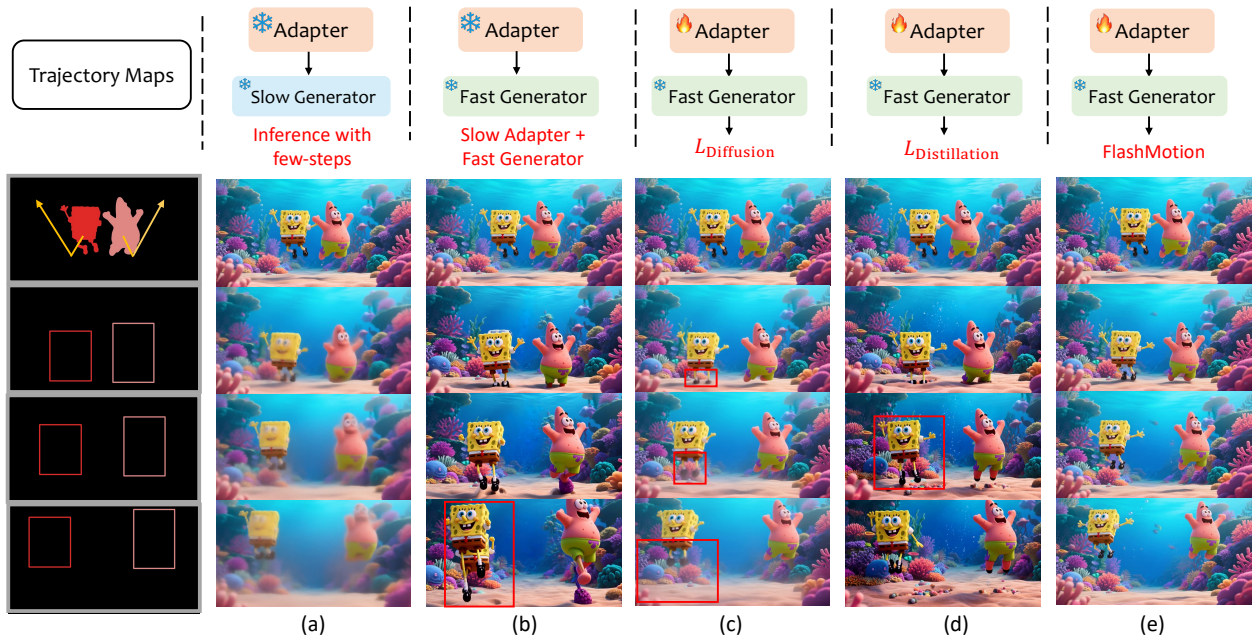


Figure 1 Illustration of the motivation and capabilities of **FlashMotion**. We define the *SlowGenerator* as the multi-step video model and the *FastGenerator* as its few-step distilled version. The *SlowAdapter* is trained with the *SlowGenerator*, while the *FastAdapter* is fine-tuned for the *FastGenerator*. (a) Using the *SlowAdapter* with *SlowGenerator* under few-step inference causes blurry outputs. (b) Applying the *SlowAdapter* to the *FastGenerator* degrades both quality and trajectory accuracy. (c) Finetuning the adapter with only diffusion loss still leads to blur artifacts. (d) Finetuning the adapter with existing distillation methods yields suboptimal quality and trajectory control. (e) **FlashMotion** achieves high-quality, accurate few-step trajectory-controllable video generation.

multi-step teacher models into few-step student models, thereby significantly accelerating video generation process [2, 13, 20, 21, 23, 33, 38, 43, 60]. However, applying these methods directly to trajectory-controllable video generation can yield suboptimal results (Fig. 1 (d)), and the acceleration of trajectory-controllable video generation still remains largely unexplored.

One straightforward way is to directly leverage existing strategies that distill a well-trained multi-step video generator (*SlowGenerator*), such as Wan [40], CogVideoX [55], etc, to a few-step student model (*FastGenerator*) while leaving the original trajectory adapter (*SlowAdapter*) unchanged. However, as shown in Fig. 1(b), this results in significant degradation in both video quality and trajectory accuracy, indicating that *SlowAdapter* is not directly compatible with *FastGenerator*. This incompatibility arises because *SlowAdapter* is tailored for the multi-step denoising process of *SlowGenerator*, where trajectory conditions slowly guide the initial noise through progressive refinement. In contrast, *FastGenerator* synthesizes videos within only a few denoising steps, resulting in totally different denoising paths.

In this paper, we propose **FlashMotion**, a novel training framework that adapts a *SlowAdapter* on top of a *FastGenerator* to achieve few-step, trajectory-controllable video generation. We observe that directly fine-tuning *SlowAdapter* to fit *FastGenerator* using a standard diffusion loss leads to reasonable trajectory alignment, but the generated videos suffer from strong blurring artifacts (Fig. 1(c)). This arises from the fact that the diffusion loss offers only pixel-level supervision without enforcing distribution-level consistency, leading to a mismatch between the generated (fake) and real data distributions.

To mitigate this issue, **FlashMotion** introduces a diffusion discriminator to guide the optimization of the trajectory adapter, bridging the gap between generated and real video distributions. Specifically, we finetune the *SlowAdapter* using a hybrid training strategy that jointly optimizes diffusion and adversarial objectives. The diffusion discriminator is trained to distinguish noisy real video latents from generated ones, thereby

aligning their underlying data distributions. Meanwhile, the diffusion loss provides pixel-level supervision, encouraging the model to produce trajectory-aligned videos. To balance the two objectives and ensure stable optimization, we further introduce a dynamic diffusion loss scaling mechanism that adaptively adjusts the loss weight during training. In addition, thanks to the strong prior provided by *SlowAdapter*, this training stage requires only a lightweight fine-tuning of 1K steps on 4 A100 GPUs, leading to minimal training cost.

Aside from the training framework, a comprehensive benchmark is also urgently needed. Existing benchmarks for trajectory-controllable video generation [18, 25, 28] are constrained by short video durations and limited trajectory annotations. To overcome these limitations, we introduce **FlashBench**, a large-scale and comprehensive benchmark that provides trajectory annotations for long video sequences. FlashBench further groups videos into six categories based on the number of foreground objects and evaluates models in each category with respect to both visual quality and trajectory control accuracy following [18]. In conclusion, our main contributions are as follows:

- To the best of our knowledge, FlashMotion is the first work to investigate few-step trajectory-controllable video generation. We propose and systematically examine a range of potentially promising approaches, offering in-depth analysis and comparison.
- We propose a novel three-stage training framework that integrates diffusion and adversarial objectives, enabling effective training of a trajectory adapter on top of a few-step video diffusion model. FlashMotion significantly accelerates video generation while simultaneously enhancing visual fidelity and trajectory accuracy.
- We present FlashBench, a large-scale benchmark comprising long video sequences with detailed trajectory annotations. Extensive experiments show that FlashMotion achieves superior performance, outperforming both few-step distillation methods and multi-step trajectory-guided video generation methods.

2 Related Works

Trajectory Controllable Video Generation Trajectory-controllable video generation has recently gained considerable attention for its capability to precisely control the motion trajectories of foreground objects during the video generation process. Some training-free methods attempt to achieve trajectory control by directly manipulating the attention map values within specific spatial regions [14, 24, 29, 54]. However, due to the lack of explicit trajectory supervision, such methods often struggle to achieve consistent and temporally coherent motion control. Recent training-based approaches introduce learnable modules for trajectory control, enabling the use of various trajectory representations as conditioning signals [4, 7, 18, 41, 42, 45–48, 56, 62, 65]. By explicitly modeling trajectory through these structured conditions, the trajectory adapter can effectively inject fine-grained spatiotemporal control into the video generation process. Despite their improved controllability, these methods still depend on multi-step diffusion inference with tens or even hundreds of denoising iterations, resulting in significant latency and computational cost. In contrast, FlashMotion proposes a few-step trajectory-controllable video generation model that drastically reduces the number of denoising iterations while preserving visual quality and trajectory controllability.

Video Diffusion Distillation Step distillation is a common and effective approach to accelerate diffusion models. Existing video distillation methods primarily adapt image distillation methods and can be broadly classified into three categories: consistency distillation, score distillation, and adversarial distillation. Consistency distillation [22, 37] enables single-step generation by directly mapping any point along the probability flow trajectory back to its origin. Methods such as VideoLCM[43], T2V-Turbo[17], and DCM[23] extend this concept to video domain, thereby achieving efficient video synthesis with minimal sampling steps. Score distillation [58, 59] focuses on minimizing the discrepancy between the score estimates of the student and teacher models. Recent video methods such as POSE [2], MagicDistillation[33], CausVid[60], and Self-Forcing[13] adopt score distillation objective, aiming to approximate the same distribution of the multi-step diffusion teacher model. Adversarial distillation[6, 31, 32] instead employs a discriminator to

narrow the distribution gap between real and generated samples. In the video domain, APT[20] and APT2 [21] leverage this strategy to perform one-step adversarial distillation, training a discriminator to distinguish real videos from those synthesized by the distilled generator. Despite their impressive efficiency gains, existing video distillation methods are not specifically designed for trajectory-controllable video generation, often resulting in degraded visual quality and trajectory accuracy when directly applied to this task.

3 Method

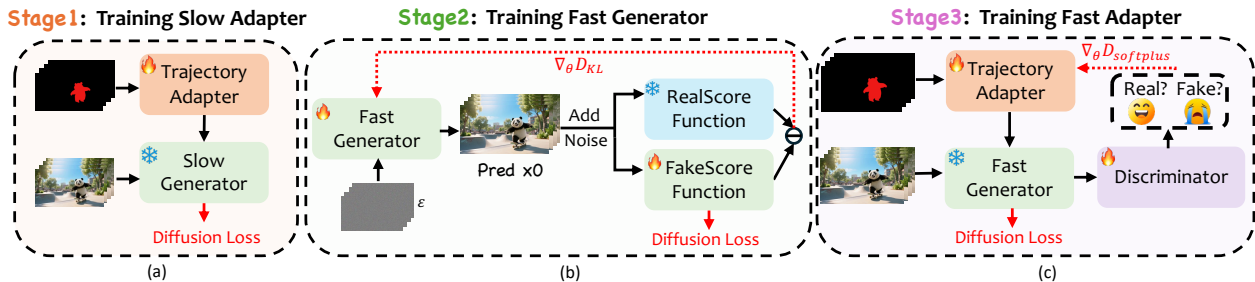


Figure 2 Overview of **FlashMotion** training pipeline. FlashMotion is trained in three stages: (1) a *SlowAdapter* is first trained on the *SlowGenerator* with a diffusion loss; (2) a *FastGenerator* is distilled from the *SlowGenerator* under the supervision of a distribution matching [59] loss; and (3) the *SlowAdapter* is finetuned to align with the *FastGenerator* using a hybrid training strategy that combines adversarial and diffusion losses.

3.1 Overview

We propose **FlashMotion**, a trajectory-controllable image-to-video framework that generates high-quality, trajectory-consistent videos in few denoising steps, achieving both controllability and efficiency. As illustrated in Fig. 2, FlashMotion achieves this goal through a three-stage training process. In Sec. 3.2, we provide a detailed explanation on training *SlowAdapter*, including its model architecture and a progressive training procedure. In Sec. 3.3, we detail the training of *FastGenerator*, which is achieved by distilling a multi-step teacher model into a few-step student model. In Sec. 3.4, we explain how we adapt the *SlowAdapter* into a *FastAdapter* via a hybrid training scheme with both diffusion and adversarial objectives. Finally, we introduce FlashBench in Sec. 3.5, which is a comprehensive benchmark tailored for evaluating long-duration video sequences.

3.2 Training Slow Adapter

As shown in Fig. 2 (a), FlashMotion first trains a trajectory adapter on *SlowGenerator* with a standard diffusion loss. We next describe its architecture and training process.

Trajectory Adapter Architecture We design two distinct trajectory adapter architectures to evaluate the generalization ability of FlashMotion: a ControlNet-based adapter [61] and a lightweight ResNet-based adapter [9]. Specifically, the number of blocks in our Trajectory Adapter is kept identical to that of the DiT [27] blocks in Wan2.2-TI2V-5B [40]. A pretrained 3D VAE [15] encoder is used to encode the trajectory maps into a latent space $Z_{trajectory} \in R^{\frac{T}{4} \times \frac{H}{16} \times \frac{W}{16} \times 48}$, which later serves as input to our Trajectory Adapter. The output from each Trajectory Adapter block is then passed through a zero-initialized convolution layer and added to the corresponding DiT block in the base model [51, 61], thereby providing trajectory guidance.

Training Procedure Following MagicMotion [18], we adopt a dense-to-sparse training strategy to progressively enhance the adapter’s trajectory understanding. The adapter is first trained with segmentation masks as dense trajectory conditions, and subsequently finetuned with bounding boxes as sparse trajectory conditions. Through this two-stage training process, we obtain the *SlowAdapter* which can provide trajectory guidance to *SlowGenerator*.

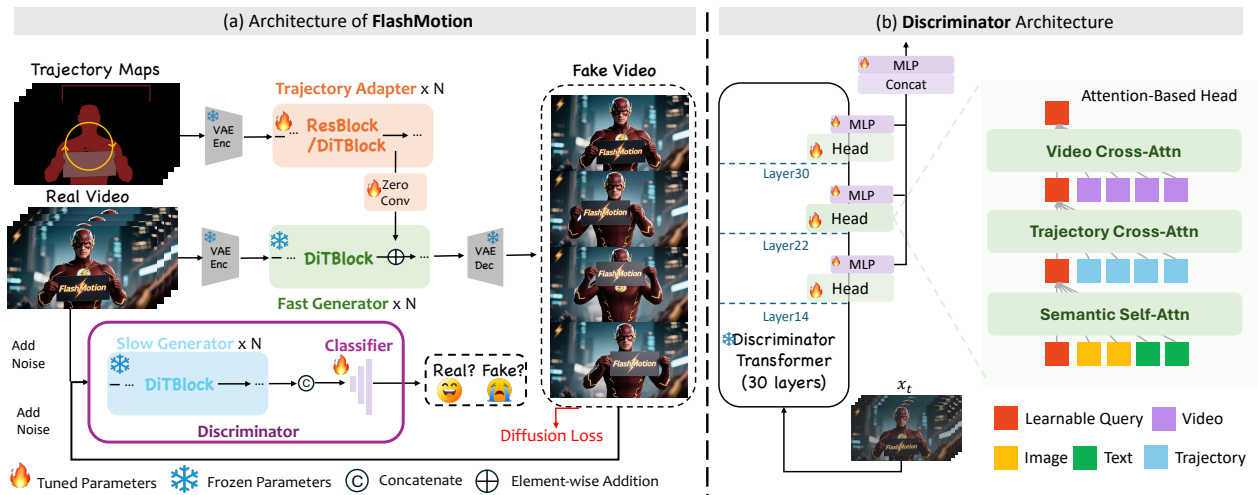


Figure 3 (a) Architecture of **FlashMotion**. The trajectory adapter is finetuned upon the *FastGenerator* with a hybrid strategy that combines both diffusion and adversarial objectives. (b) Detailed illustration of our diffusion discriminator architecture. The discriminator adopts a DiT backbone cloned from the *SlowGenerator*, while several intermediate features from its DiT blocks are fed into an attention-based classifier to distinguish real videos from generated ones.

3.3 Training Fast Generator

We aim to distill *SlowGenerator* into a *FastGenerator* that can generate high quality video sequences within only a few denoising steps. Specifically, we adopt Wan2.2-TI2V-5B [40] as our *SlowGenerator*, which is built upon the DiT [27] architecture and employs a stack of transformer [39] blocks for iterative denoising.

For distillation, we employ DMD [59], a score distillation method that aligns the teacher and student video distributions p_{real} and p_{fake} by minimizing their Kullback–Leibler (KL) divergence. We here consider three components: a few-step student generator G_{θ} , a real score model μ_{real} , and a fake score model μ_{fake} , all initialized from the weights of Wan2.2-TI2V-5B [40]. As shown in Fig. 2(b), We first perform a few-step inference process with G_{θ} which maps pure Gaussian noise $\epsilon \sim \mathcal{N}(0, I)$ to clean video samples x_0 . These clean samples are subsequently perturbed with additive Gaussian noise of varying magnitudes to produce diffused videos x_t . These perturbed samples are then passed to the real score model μ_{real} and the fake score model μ_{fake} , which respectively estimate the scores of the real and generated video distributions, defined as $s_{\text{real}}x_t, t = \nabla_x \log p_{\text{real}}x_t, t, s_{\text{fake}}x_t, t = \nabla_x \log p_{\text{fake}}x_t, t$.

Finally, our student generator model G_{θ} can be updated by the following distribution matching gradient:

$$\begin{aligned} \nabla \mathcal{L}_{\text{DMD}} &= \mathbb{E}_t (\nabla_{\theta} \text{KL} (p_{\text{fake}} \| p_{\text{real}})) \\ &= \mathbb{E}_{\epsilon \sim \mathcal{N}(0; I)} \left[- (s_{\text{real}} (x_t, t) - s_{\text{fake}} (x_t, t)) \frac{dG_{\theta}}{d\theta} \right] \end{aligned} \quad (1)$$

During training, we freeze the real score model μ_{real} as the target distribution. Besides, we dynamically update the fake score model μ_{fake} by minimizing a standard diffusion loss, to track the evolving sample distribution produced by the student generator G_{θ} .

$$\mathcal{L}_{\text{fake}} = \mathbb{E} \left[\|\mu_{\text{fake}}x_t, t - x_0\|_2^2 \right] \quad (2)$$

where x_0 denotes the fake video samples generated by G_{θ} .

3.4 Training Fast Adapter

As shown in Fig. 1(b), directly using the *SlowAdapter* upon the *FastGenerator* can lead to degraded visual quality and poor trajectory accuracy. Thus, there is an urgent need for a simple and effective approach to fine-tune the *SlowAdapter* into a *FastAdapter*. We adopt an hybrid training scheme that combines diffusion objectives and an adversarial objective, allowing the model to maintain trajectory accuracy and avoid visual quality degradation (Fig. 2(c)).

Diffusion loss We begin by initializing the weights of the trajectory adapter using the parameters of *SlowAdapter* trained in Stage 1 (see Sec. 3.2 for details). During training, as shown in Fig. 3 (a), a pretrained 3D VAE encoder [40] maps both the trajectory map and the real video into a latent space, denoted as z_{traj} and x_0^{real} , which then serves as the input to the trajectory adapter and the video generator. The trajectory features produced by each adapter block are injected into the corresponding block of the fast generator through a zero-initialized convolutional layer, thereby guiding the generation of the synthesized (fake) video latents $x_0^{\text{fake}} = G_\theta x_t, t$. We then optimize the trajectory adapter using a standard diffusion loss:

$$\mathcal{L}_{diffusion} = \left\| G_\theta x_t, t - x_0^{\text{real}} \right\|_2^2 \quad (3)$$

Adversarial Training However, as shown in Fig. 1(c), finetuning the *SlowAdapter* solely with the diffusion loss often leads to noticeable blurry artifacts in the generated videos. Since the diffusion loss only enforces pixel-level alignment, it leads to a mismatch between the distributions of real and generated videos. To this end, we introduce a diffusion discriminator to bridge this distribution gap.

Inspired by APT [20], we use a diffused version of the real and fake video latents, denoted as x_t^{fake} and x_t^{real} , as input to the diffusion discriminator, which is trained to produce a logit that effectively distinguishes between the real and generated (fake) videos. We initialize the discriminator backbone using the weight of Wan2.2-TI2V-5B [40], and incorporate an attention-based classifier into the diffusion transformer to produce logits. For memory efficiency and faster convergence, we freeze the backbone of the diffusion discriminator and only train the newly added classifier.

As shown in Fig. 3 (b), the classifiers are attached to selected layers of the original DiT backbone. Each classifier includes an attention-based head followed by an MLP layer that outputs a single token. The tokens from all classifiers are then concatenated and passed through another MLP layer to produce the final logits, indicating whether the input video is real or fake.

Specifically, as illustrated in Fig. 3 (b), each classifier block processes a learnable query token through three consecutive attention layers. The *Semantic Self-Attention* layer integrates the first-frame image and text information to enhance semantic representation. In this layer, the learnable query token q is concatenated with the first-frame image embeddings e_i and text embeddings e_{text} , and then processed by a self-attention operation that enables the query token to attend across multiple semantic modalities. Then, the resulting token is subsequently passed to the *Trajectory Cross-Attention* layer, where it serves as the query and attends to the trajectory map tokens e_{traj} , used as keys and values in the attention computation [39]. Finally, the token is processed by the *Video Cross-Attention* layer, attending to the video tokens e_{video} . Each attention layer is followed by a residual connection applied to the learnable token, which is omitted in Fig. 3 (b) for clarity.

We thus employ the following loss to finetune the trajectory adapter and the diffusion discriminator in an alternating scheme.

$$\mathcal{L}_{\mathcal{G}} = \min_{\theta} \mathbb{E}_{t \sim 0, T} \left[f \left(-\mathcal{D}_{\phi} \left(x_t^{\text{fake}}, t \right) \right) \right] \quad (4)$$

$$\mathcal{L}_{\mathcal{D}} = \min_{\phi} \mathbb{E}_{t \sim 0, T} \left[f \left(-\mathcal{D}_{\phi} \left(x_t^{\text{real}}, t \right) \right) f \left(\mathcal{D}_{\phi} \left(x_t^{\text{fake}}, t \right) \right) \right] \quad (5)$$

where f is the softplus function [3], $T = 1000$, \mathcal{D}_{ϕ} denotes the diffusion discriminator, θ and ϕ represent the parameters of the trajectory adapter and classifier.

Dynamic Diffusion Loss Scale The diffusion loss enforces the generated video to follow the user-specified trajectory at the pixel level, while the GAN loss bridges the distribution gap between the generated and real videos. Accordingly, we jointly train the trajectory adapter using a combination of these two objectives, formulated as:

$$\mathcal{L} = \mathcal{L}_{\mathcal{G}} + \lambda \mathcal{L}_{diffusion} \quad (6)$$

However, we observe that in the early stages of training, the gradients of the diffusion loss $\mathcal{L}_{diffusion}$ are substantially larger than those of the GAN loss $\mathcal{L}_{\mathcal{G}}$, and directly combining them can still lead to blurred results. To mitigate this imbalance, we introduce a dynamic weighting scheme for the coefficient λ , defined as:

$$\lambda = \frac{1}{4} \times 10^{-3} \times step \quad (7)$$

where *step* means the current training iteration.

3.5 FlashBench

Previous works on trajectory-controllable video generation [18, 19, 26, 34, 44, 49, 62, 65] have primarily been evaluated on DAVIS [28], VIPSeg [25], and MagicBench [18]. While existing benchmarks focus on short video sequences, FlashMotion is capable of generating videos up to 121 frames long. This discrepancy prevents a thorough evaluation of the long-term temporal consistency and trajectory controllability of FlashMotion. Therefore, there is an urgent need for a publicly available benchmark that targets long-sequence trajectory-controllable video generation.

Following the data pipeline introduced in MagicMotion [18], we build FlashBench by extending MagicBench with comprehensive trajectory annotations for all frames. To facilitate detailed analysis, FlashBench is further organized into six groups based on the number of foreground objects, ranging from one to five, and more than five.

4 Experiment

We first introduce the experimental settings, including the datasets, implementation details, evaluation metrics, and comparison baselines in Sec. 4.1. Then, Sec. 4.2 reports quantitative and qualitative results, conducting comprehensive comparisons with existing methods. Finally, Sec. 4.3 provides ablation studies that further analyze the contribution and effectiveness of each component of FlashMotion.

4.1 Experiment Settings

Datasets. We use MagicData [18] as our training dataset for all the three training stages, which contains 23K high quality videos with both text and trajectory annotations, including segmentation masks and bounding boxes. For evaluation, we conduct experiments on three different benchmarks: FlashBench, MagicBench [18] and DAVIS [28].

Implementation details. In Stage1, we adopt two architectures for the trajectory adapter: ResNet [10] and ControlNet [61]. The ResNet adapter is trained from scratch, while the ControlNet adapter is initialized from the main DiT weights. Both are first trained for 4.6K steps using segmentation masks as trajectory conditions, and then fine-tuned for another 5.4K steps with bounding boxes. Training is conducted on 16 A100 GPUs with a batch size of 1 per GPU and a learning rate of 2×10^{-6} . In Stage 2, *FastGenerator* is obtained by distilling Wan2.2-TI2V-5B [40] into a four-step image-to-video generator. All parameters are fine-tuned for 5.5K steps on 16 A100 GPUs with a batch size of 1 per GPU. During training, the generator and fake score model are optimized with learning rates of 5×10^{-7} and 1×10^{-7} , respectively, following a 1:5 update schedule. In Stage 3, the trajectory adapter and discriminator are optimized with a learning rate of 2×10^{-6} also under a 1:5 update ratio. The diffusion loss scale is gradually increased according to $\lambda = \frac{1}{4} \times 10^{-3} \times step$ 0.1, where *step* denotes the current training iteration. This stage is trained for 1K steps on 4 A100 GPUs with a batch size of 1 per GPU.

Table 1 Quantitative results on **FlashBench**, **MagicBench**, and **DAVIS**. We report FID, FVD, and mask/box IoU (%) for both ResNet and ControlNet adapters. For each metric, the best result is highlighted in **bold**, and the second best is underlined. Denoising time is measured for generating 121 frames on one A100 GPU.

Methods	FlashBench			MagicBench			DAVIS			Denoising Time (s)	Params (B)	
	FID(↓)	FVD(↓)	M/B IoU(↑)	FID(↓)	FVD(↓)	M/B IoU(↑)	FID(↓)	FVD(↓)	M/B IoU(↑)			
MultiSteps (50 Steps)												
MagicMotion [18]	20.03	138.83	<u>68.10/73.68</u>	15.17	<u>107.21</u>	<u>76.61/81.45</u>	50.36	760.95	<u>53.94/72.84</u>	1158.63	11.53	
Wan2.2 (ResNet) [40]	19.03	139.61	52.19/57.76	21.72	140.41	62.09/67.85	46.44	<u>703.15</u>	31.22/42.74	333.00	5.02	
Wan2.2 (ControlNet) [40]	16.93	152.04	65.41/71.28	20.05	157.98	72.80/78.46	43.70	791.80	52.76/71.20	664.53	10.28	
DragAnything [49]	34.93	267.56	58.54/61.72	31.36	253.40	66.30/70.85	70.70	1166.22	40.13/53.60	589.07	2.21	
SG-I2V [26]	28.52	252.49	50.20/55.72	32.60	168.82	68.78/74.39	90.93	1170.60	37.36/50.96	1277.15	1.52	
Tora [62]	31.79	315.11	48.17/53.70	26.27	245.23	58.95/64.03	51.75	766.76	37.98/50.90	691.13	6.32	
LeviTor [41]	64.58	335.47	36.36/39.81	38.32	194.53	39.96/46.36	97.98	922.68	25.24/31.42	80.08	2.21	
FewSteps (4 Steps) — Adapter: ResNet												
DMD [58]	24.38	228.33	43.24/52.61	25.27	206.57	49.69/59.44	51.75	1058.35	33.08/49.78	11.72	5.02	
GAN [6]	31.32	208.06	43.78/49.99	33.31	209.93	56.60/63.10	66.31	1143.14	30.49/42.80	11.72	5.02	
LCM [22]	26.79	462.09	55.31/60.80	28.24	398.06	64.98/70.83	63.07	1075.61	42.56/58.52	11.72	5.02	
FlashMotion	<u>15.81</u>	<u>108.96</u>	63.96/70.01	<u>14.16</u>	109.20	72.34/77.92	50.58	786.42	46.74/64.00	11.72	5.02	
FewSteps (4 Steps) — Adapter: ControlNet												
DMD [58] / GAN [6]											OOM	-
LCM [22]	28.34	340.29	61.29/64.83	25.87	261.87	70.55/74.57	62.25	1164.75	45.94/61.27	24.44	10.28	
FlashMotion	14.35	96.08	69.15/75.38	12.49	99.30	76.92/82.17	<u>45.66</u>	690.13	54.54/74.37	24.44	10.28	

Evaluation Metrics. For evaluation, we follow prior works [18, 41, 45, 49, 65] and adopt FID [11] and FVD [30] to measure visual quality. Besides, we follow MagicMotion [18] and employ Mask_IoU and Box_IoU to quantify the trajectory accuracy.

Comparison Baselines. FlashMotion is evaluated against several state-of-the-art trajectory-controllable video generation methods, including MagicMotion [18], Tora [62], DragAnything [49], SGI2V [26], LeviTor [41], and Wan2.2-TI2V-5B [40] combined with the *SlowAdapter*. Since no existing methods support few-step trajectory-controllable video generation, we design several baselines based on existing video distillation methods [6, 22, 58] for comparison. In these methods, we define the teacher model as the *SlowAdapter* combined with the *SlowGenerator*, while the student model consists of the adapter paired with the *FastGenerator*. Since DMD [58] and GAN [6] cause CUDA OOM errors under the ControlNet architecture, we report their results only with ResNet.

4.2 Comparison with Other Approaches

Quantitative comparison

We compare FlashMotion with existing methods on FlashBench, MagicBench [18], and DAVIS [28], evaluating both visual quality and trajectory accuracy. In FlashBench, we use the first 121 frames of each video as the ground-truth. Since several prior methods [18, 41, 49, 62] cannot generate videos of this length, we uniformly sample N frames from these 121 frames, where N corresponds to the maximum video length each method supports. In MagicBench [18] and DAVIS [28], we use the first 49 frames of each generated video for evaluation following MagicMotion [18]. As shown in Tab. 1, FlashMotion outperforms all existing few-step distillation methods [6, 22, 58] in both visual quality and trajectory accuracy across different adapter architectures. When equipped with ControlNet as the adapter, FlashMotion further outperforms all prior multi-step baselines while retaining the efficiency of few-step sampling, achieving a 47× speedup over the previous SOTA [18].

Qualitative comparison

The Qualitative comparison results are presented in Fig. 4, along with the corresponding input image, prompt, and trajectory. We include visualizations of all few-step baselines and four representative DiT-based multi-step baselines, MagicMotion[18], Tora [62] and Wan [40] + *SlowGenerator*. As shown in Fig. 4, FlashMotion



Figure 4 Qualitative Comparisons results. FlashMotion demonstrates superior qualitative performance, outperforming both previous multi-step trajectory-controllable methods and few-step distillation baselines.

outperforms all these methods on both visual quality and trajectory accuracy.

4.3 Ablation Studies

Due to limited space, we only present ablation results on FlashBench here in the main paper, please refer to supplementary materials for more results on MagicBench [18] and DAVIS [28]. For fair comparison, all experiments follow the same training configurations as FlashMotion Stage3.

Fast Adapter. To verify the necessity of the *FastAdapter*, we compute the quantitative performance of directly applying the *SlowAdapter* to the *FastGenerator*. As shown in Table. 2, removing the *FastAdapter* training stage leads to a notable degradation in both visual quality and trajectory accuracy. The result in Fig. 5 also shows that removing this training stage can cause severe color shift in videos. This demonstrates that *SlowAdapter* cannot directly control the generation process of *FastGenerator*, highlighting the necessity of the *FastAdapter* training stage.

Diffusion Loss. We evaluate the effect of the diffusion loss by removing it during training. As shown in Table. 2 and Fig. 5, without the diffusion loss, the generated videos exhibit significantly lower trajectory accuracy, showing clear misalignment between the generated videos and the user-provided trajectories. Moreover, removing the diffusion loss can also lead to decline in visual quality.

GAN Loss. We perform an ablation study on the GAN loss, as shown in Table 2. While removing the adversarial objectives slightly improves trajectory accuracy, it causes a drastic drop of nearly 90% in visual

Table 2 Ablation studies on the *FastAdapter* training stage, diffusion loss, GAN loss, and the dynamic loss scaling strategy.

Methods	FID↓	FVD↓	M IoU↑	B IoU↑
<i>Adapter Type: ResNet</i>				
Slow Adapter	22.75	168.46	49.79	56.62
w/o Diffusion Loss	18.87	161.07	52.04	58.04
w/o GAN Loss	22.74	206.75	65.82	70.60
w/o Dynamic Scale	26.32	210.93	65.54	69.77
FlashMotion	15.81	108.96	63.96	70.01
<i>Adapter Type: ControlNet</i>				
Slow Adapter	19.44	171.83	62.72	69.38
w/o Diffusion Loss	21.21	172.04	55.91	61.59
w/o GAN Loss	28.82	265.46	71.56	75.48
w/o Dynamic Scale	19.93	155.55	70.46	75.89
FlashMotion	14.35	96.08	69.15	75.38

quality, introducing severe blurring artifacts as illustrated in Fig. 5.

Dynamic Diffusion Loss Scaling. We further evaluate the effectiveness of our dynamic diffusion loss scaling strategy by fixing the loss scale to 1 during training. As reported in Table 2, disabling the dynamic scaling mechanism leads to a noticeable decline in visual quality, again resulting in significant blurring artifacts as shown in Fig. 5. **Discriminator Architecture.** To validate the design of our discriminator, we conduct experiments on four different discriminator architectures. As shown in Table 3, using only the *Video Cross-Attention* layer yields the worst visual quality and trajectory accuracy. In contrast, incorporating the *Semantic Self-Attention* module improves the model’s semantic understanding, thereby enhancing the visual quality of the generated videos, while the *Trajectory Cross-Attention* module effectively strengthens trajectory control accuracy. Our full discriminator architecture achieves the best performance across all metrics.

Table 3 Ablation study on the discriminator architecture on **FlashBench**. VC denotes the Video Cross-Attention layer, SS denotes the Semantic Self-Attention layer, and TC denotes the Trajectory Cross-Attention layer.

Methods	FID(↓)	FVD(↓)	M IoU(↑)	B IoU(↑)
Adapter Type: ResNet				
VC only	16.76	110.83	62.07	67.76
SS+VC	16.31	109.02	62.54	68.05
TC+VC	16.64	110.01	62.99	69.36
FlashMotion	15.81	108.96	63.96	70.01
Adapter Type: ControlNet				
VC only	15.56	115.72	63.04	71.73
SS+VC	15.37	99.24	65.84	72.35
TC+VC	15.70	101.06	68.78	73.85
FlashMotion	14.35	96.08	69.15	75.38

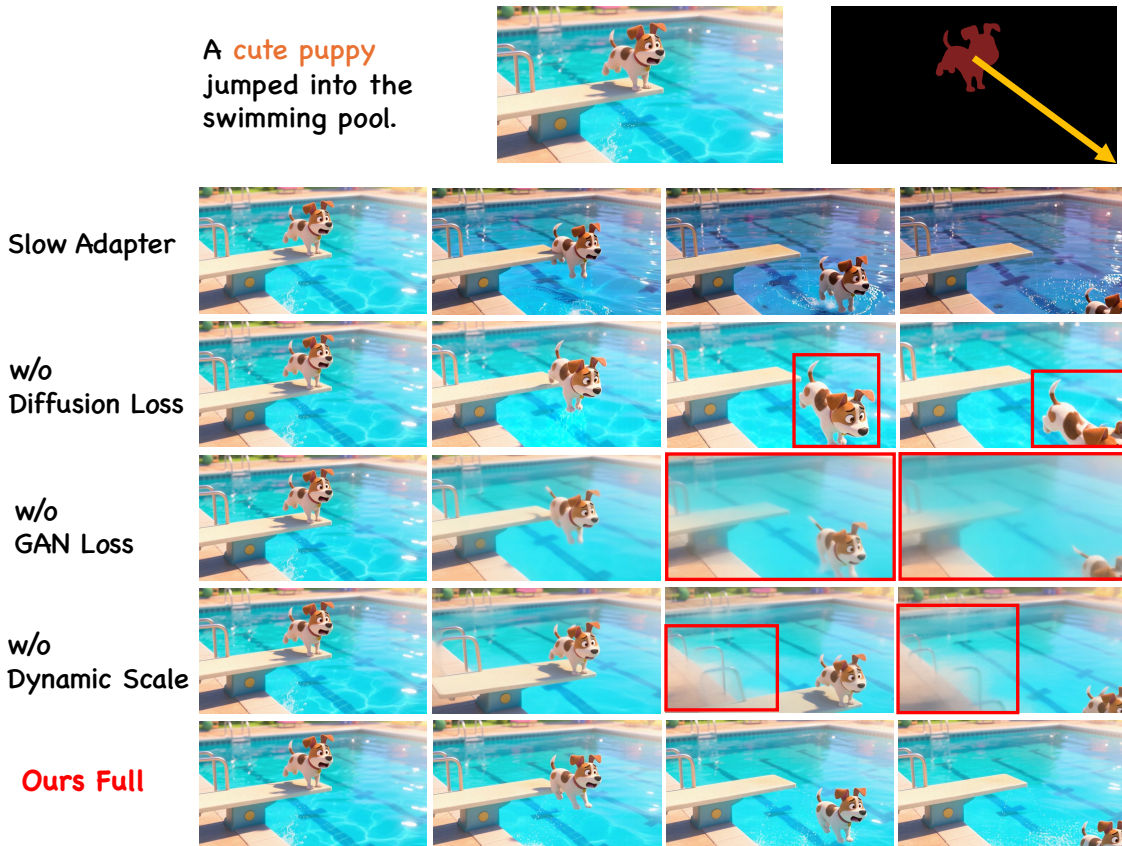


Figure 5 Ablation studies on the *FastAdapter* training stage, diffusion loss, GAN loss, and the dynamic loss scaling strategy.

5 Conclusion

In this work, we introduce FlashMotion, a novel framework that achieves few-step trajectory-controllable video generation through a three-stage training paradigm. First, we train a trajectory adapter on a multi-step video generator to enable precise trajectory control. Next, we distill the multi-step generator into a few-step version to accelerate video synthesis. Finally, we finetune the trajectory adapter using a hybrid strategy that combines diffusion and adversarial objectives, aligning it with the few-step generator to achieve few-step trajectory-controllable video generation. In addition, we present FlashBench, a comprehensive benchmark designed for long-sequence trajectory-controllable video generation, evaluating both visual quality and trajectory accuracy. Extensive experiments demonstrate that FlashMotion not only surpasses existing few-step distillation approaches but also outperforms prior multi-step trajectory-controllable video generation models in both visual fidelity and trajectory consistency.

Acknowledge This work was supported by National Natural Science Foundation of China (No. 62472098) and the Science and Technology Commission of Shanghai Municipality (No. 25511106100).

References

- [1] Andreas Blattmann, Tim Dockhorn, Sumith Kulal, Daniel Mendelevitch, Maciej Kilian, Dominik Lorenz, Yam Levi, Zion English, Vikram Voleti, Adam Letts, et al. Stable video diffusion: Scaling latent video diffusion models to large datasets. [arXiv preprint arXiv:2311.15127](#), 2023.
- [2] Jiayang Cheng, Bing Ma, Xuhua Ren, Hongyi Jin, Kai Yu, Peng Zhang, Wenyue Li, Yuan Zhou, Tianxiang Zheng, and Qinglin Lu. Pose: Phased one-step adversarial equilibrium for video diffusion models. [arXiv preprint arXiv:2508.21019](#), 2025.
- [3] Charles Dugas, Yoshua Bengio, François Bédille, Claude Nadeau, and René Garcia. Incorporating second-order functional knowledge for better option pricing. In T. Leen, T. Dietterich, and V. Tresp, editors, [Advances in Neural Information Processing Systems](#), 2000.
- [4] Xiao Fu, Xian Liu, Xintao Wang, Sida Peng, Menghan Xia, Xiaoyu Shi, Ziyang Yuan, Pengfei Wan, Di Zhang, and Dahua Lin. 3dtrajmaster: Mastering 3d trajectory for multi-entity motion in video generation. In [ICLR](#), 2025.
- [5] Daniel Geng, Charles Herrmann, Junhwa Hur, Forrester Cole, Serena Zhang, Tobias Pfaff, Tatiana Lopez-Guevara, Carl Doersch, Yusuf Aytar, Michael Rubinstein, Chen Sun, Oliver Wang, Andrew Owens, and Deqing Sun. Motion prompting: Controlling video generation with motion trajectories. [arXiv preprint arXiv:2412.02700](#), 2024.
- [6] Ian Goodfellow, Jean Pouget-Abadie, Mehdi Mirza, Bing Xu, David Warde-Farley, Sherjil Ozair, Aaron Courville, and Yoshua Bengio. Generative adversarial nets. [NeurIPS](#), 2014.
- [7] Zekai Gu, Rui Yan, Jiahao Lu, Peng Li, Zhiyang Dou, Chenyang Si, Zhen Dong, Qifeng Liu, Cheng Lin, Ziwei Liu, Wenping Wang, and Yuan Liu. Diffusion as shader: 3d-aware video diffusion for versatile video generation control. [arXiv preprint arXiv:2501.03847](#), 2025.
- [8] Yoav HaCohen, Nisan Chiprut, Benny Brazowski, Daniel Shalem, Dudu Moshe, Eitan Richardson, Eran Levin, Guy Shiran, Nir Zabari, Ori Gordon, Poriya Panet, Sapir Weissbuch, Victor Kulikov, Yaki Bitterman, Zeev Melumian, and Ofir Bibi. Ltx-video: Realtime video latent diffusion. [arXiv preprint arXiv:2501.00103](#), 2024.
- [9] Kaiming He, Xiangyu Zhang, Shaoqing Ren, and Jian Sun. Deep residual learning for image recognition. In [CVPR](#), 2016.
- [10] Kaiming He, Xiangyu Zhang, Shaoqing Ren, and Jian Sun. Deep residual learning for image recognition. In [Proceedings of the IEEE conference on computer vision and pattern recognition](#), 2016.
- [11] Martin Heusel, Hubert Ramsauer, Thomas Unterthiner, Bernhard Nessler, and Sepp Hochreiter. Gans trained by a two time-scale update rule converge to a local nash equilibrium. [NeurIPS](#), 2017.
- [12] Jonathan Ho, Ajay Jain, and Pieter Abbeel. Denoising diffusion probabilistic models. [NeurIPS](#), 2020.
- [13] Xun Huang, Zhengqi Li, Guande He, Mingyuan Zhou, and Eli Shechtman. Self forcing: Bridging the train-test gap in autoregressive video diffusion. [arXiv preprint arXiv:2506.08009](#), 2025.

- [14] Yash Jain, Anshul Nasery, Vibhav Vineet, and Harkirat Behl. Peekaboo: Interactive video generation via masked-diffusion. arXiv preprint arXiv:2312.07509, 2023.
- [15] Diederik P Kingma and Max Welling. Auto-encoding variational bayes. arXiv preprint arXiv:1312.6114, 2013.
- [16] Weijie Kong, Qi Tian, Zijian Zhang, Rox Min, Zuozhuo Dai, Jin Zhou, Jiangfeng Xiong, Xin Li, Bo Wu, Jianwei Zhang, et al. Hunyuanvideo: A systematic framework for large video generative models. arXiv preprint arXiv:2412.03603, 2024.
- [17] Jiachen Li, Weixi Feng, Tsu-Jui Fu, Xinyi Wang, Sugato Basu, Wenhui Chen, and William Yang Wang. T2v-turbo: Breaking the quality bottleneck of video consistency model with mixed reward feedback. Advances in neural information processing systems, 2024.
- [18] Quanhao Li, Zhen Xing, Rui Wang, Hui Zhang, Qi Dai, and Zuxuan Wu. Magicmotion: Controllable video generation with dense-to-sparse trajectory guidance. In ICCV, 2025.
- [19] Yaowei Li, Xintao Wang, Zhaoyang Zhang, Zhouxia Wang, Ziyang Yuan, Liangbin Xie, Ying Shan, and Yuexian Zou. Image conductor: Precision control for interactive video synthesis. In AAAI, 2025.
- [20] Shanchuan Lin, Xin Xia, Yuxi Ren, Ceyuan Yang, Xuefeng Xiao, and Lu Jiang. Diffusion adversarial post-training for one-step video generation. arXiv preprint arXiv:2501.08316, 2025.
- [21] Shanchuan Lin, Ceyuan Yang, Hao He, Jianwen Jiang, Yuxi Ren, Xin Xia, Yang Zhao, Xuefeng Xiao, and Lu Jiang. Autoregressive adversarial post-training for real-time interactive video generation. arXiv preprint arXiv:2506.09350, 2025.
- [22] Simian Luo, Yiqin Tan, Longbo Huang, Jian Li, and Hang Zhao. Latent consistency models: Synthesizing high-resolution images with few-step inference. arXiv preprint arXiv:2310.04378, 2023.
- [23] Zhengyao Lv, Chenyang Si, Tianlin Pan, Zhaoxi Chen, Kwan-Yee K Wong, Yu Qiao, and Ziwei Liu. Dcm: Dual-expert consistency model for efficient and high-quality video generation. arXiv preprint arXiv:2506.03123, 2025.
- [24] Wan-Duo Kurt Ma, John P Lewis, and W Bastiaan Kleijn. Trailblazer: Trajectory control for diffusion-based video generation. In SIGGRAPH Asia 2024 Conference Papers, 2024.
- [25] Jiayu Miao, Yunchao Wei, Yu Wu, Chen Liang, Guangrui Li, and Yi Yang. Vspw: A large-scale dataset for video scene parsing in the wild. In CVPR, 2021.
- [26] Koichi Namekata, Sherwin Bahmani, Ziyi Wu, Yash Kant, Igor Gilitschenski, and David B. Lindell. Sg-i2v: Self-guided trajectory control in image-to-video generation. In ICLR, 2025. URL <https://openreview.net/forum?id=uQjySppU9x>.
- [27] William Peebles and Saining Xie. Scalable diffusion models with transformers. arXiv preprint arXiv:2212.09748, 2022.
- [28] F. Perazzi, J. Pont-Tuset, B. McWilliams, L. Van Gool, M. Gross, and A. Sorkine-Hornung. A benchmark dataset and evaluation methodology for video object segmentation. In CVPR, 2016.
- [29] Haonan Qiu, Zhaoxi Chen, Zhouxia Wang, Yingqing He, Menghan Xia, and Ziwei Liu. Freetraj: Tuning-free trajectory control in video diffusion models. arXiv preprint arXiv:2406.16863, 2024.
- [30] René Ranftl, Katrin Lasinger, David Hafner, Konrad Schindler, and Vladlen Koltun. Towards robust monocular depth estimation: Mixing datasets for zero-shot cross-dataset transfer. TPAMI, 2020.
- [31] Axel Sauer, Frederic Boesel, Tim Dockhorn, Andreas Blattmann, Patrick Esser, and Robin Rombach. Fast high-resolution image synthesis with latent adversarial diffusion distillation. In SIGGRAPH Asia 2024 Conference Papers, 2024.
- [32] Axel Sauer, Dominik Lorenz, Andreas Blattmann, and Robin Rombach. Adversarial diffusion distillation. In European Conference on Computer Vision, 2024.
- [33] Shitong Shao, Hongwei Yi, Hanzhong Guo, Tian Ye, Daquan Zhou, Michael Lingelbach, Zhiqiang Xu, and Zeke Xie. Magicdistillation: Weak-to-strong video distillation for large-scale few-step synthesis. arXiv preprint arXiv:2503.13319, 2025.

- [34] Xiaoyu Shi, Zhaoyang Huang, Fu-Yun Wang, Weikang Bian, Dasong Li, Yi Zhang, Manyuan Zhang, Ka Chun Cheung, Simon See, Hongwei Qin, et al. Motion-i2v: Consistent and controllable image-to-video generation with explicit motion modeling. SIGGRAPH, 2024.
- [35] Jiaming Song, Chenlin Meng, and Stefano Ermon. Denoising diffusion implicit models. arXiv preprint arXiv:2010.02502, 2020.
- [36] Yang Song, Jascha Sohl-Dickstein, Diederik P Kingma, Abhishek Kumar, Stefano Ermon, and Ben Poole. Score-based generative modeling through stochastic differential equations. arXiv preprint arXiv:2011.13456, 2020.
- [37] Yang Song, Prafulla Dhariwal, Mark Chen, and Ilya Sutskever. Consistency models. arXiv preprint arXiv:2303.01469, 2023.
- [38] Yanxiao Sun, Jiafu Wu, Yun Cao, Chengming Xu, Yabiao Wang, Weijian Cao, Donghao Luo, Chengjie Wang, and Yanwei Fu. Swiftvideo: A unified framework for few-step video generation through trajectory-distribution alignment. arXiv preprint arXiv:2508.06082, 2025.
- [39] Ashish Vaswani, Noam Shazeer, Niki Parmar, Jakob Uszkoreit, Llion Jones, Aidan N Gomez, Łukasz Kaiser, and Illia Polosukhin. Attention is all you need. NeurIPS, 2017.
- [40] Team Wan, Ang Wang, Baole Ai, Bin Wen, Chaojie Mao, Chen-Wei Xie, Di Chen, Feiwu Yu, Haiming Zhao, Jianxiao Yang, Jianyuan Zeng, Jiayu Wang, Jingfeng Zhang, Jingren Zhou, Jinkai Wang, Jixuan Chen, Kai Zhu, Kang Zhao, Keyu Yan, Lianghua Huang, Mengyang Feng, Ningyi Zhang, Pandeng Li, Pingyu Wu, Ruihang Chu, Ruili Feng, Shiwei Zhang, Siyang Sun, Tao Fang, Tianxing Wang, Tianyi Gui, Tingyu Weng, Tong Shen, Wei Lin, Wei Wang, Wei Wang, Wenmeng Zhou, Wenten Wang, Wenting Shen, Wenyuan Yu, Xianzhong Shi, Xiaoming Huang, Xin Xu, Yan Kou, Yangyu Lv, Yifei Li, Yijing Liu, Yiming Wang, Yingya Zhang, Yitong Huang, Yong Li, You Wu, Yu Liu, Yulin Pan, Yun Zheng, Yuntao Hong, Yupeng Shi, Yutong Feng, Zeyinzi Jiang, Zhen Han, Zhi-Fan Wu, and Ziyu Liu. Wan: Open and advanced large-scale video generative models. arXiv preprint arXiv:2503.20314, 2025.
- [41] Hanlin Wang, Hao Ouyang, Qiuyu Wang, Wen Wang, Ka Leong Cheng, Qifeng Chen, Yujun Shen, and Limin Wang. Levitor: 3d trajectory oriented image-to-video synthesis. In CVPR, pages 12490–12500, 2025.
- [42] Qinghe Wang, Yawen Luo, Xiaoyu Shi, Xu Jia, Huchuan Lu, Tianfan Xue, Xintao Wang, Pengfei Wan, Di Zhang, and Kun Gai. Cinemaster: A 3d-aware and controllable framework for cinematic text-to-video generation. In SIGGRAPH, 2025.
- [43] Xiang Wang, Shiwei Zhang, Han Zhang, Yu Liu, Yingya Zhang, Changxin Gao, and Nong Sang. Videolcm: Video latent consistency model. arXiv preprint arXiv:2312.09109, 2023.
- [44] Zhouxia Wang, Yushi Lan, Shangchen Zhou, and Chen Change Loy. ObjCtrl-2.5D: Training-free object control with camera poses. In arXiv preprint arXiv:2412.07721, 2024.
- [45] Zhouxia Wang, Ziyang Yuan, Xintao Wang, Yaowei Li, Tianshui Chen, Menghan Xia, Ping Luo, and Ying Shan. Motionctrl: A unified and flexible motion controller for video generation. In SIGGRAPH, 2024.
- [46] Yujie Wei, Shiwei Zhang, Zhiwu Qing, Hangjie Yuan, Zhiheng Liu, Yu Liu, Yingya Zhang, Jingren Zhou, and Hongming Shan. Dreamvideo: Composing your dream videos with customized subject and motion. In Proceedings of the IEEE/CVF Conference on Computer Vision and Pattern Recognition, 2024.
- [47] Yujie Wei, Shiwei Zhang, Hangjie Yuan, Xiang Wang, Haonan Qiu, Rui Zhao, Yutong Feng, Feng Liu, Zhizhong Huang, Jiabin Ye, et al. Dreamvideo-2: Zero-shot subject-driven video customization with precise motion control. arXiv preprint arXiv:2410.13830, 2024.
- [48] Yujie Wei, Shiwei Zhang, Hangjie Yuan, Biao Gong, Longxiang Tang, Xiang Wang, Haonan Qiu, Hengjia Li, Shuai Tan, Yingya Zhang, et al. Dreamrelation: Relation-centric video customization. In Proceedings of the IEEE/CVF International Conference on Computer Vision, 2025.
- [49] Weijia Wu, Zhuang Li, Yuchao Gu, Rui Zhao, Yefei He, David Junhao Zhang, Mike Zheng Shou, Yan Li, Tingting Gao, and Di Zhang. Draganything: Motion control for anything using entity representation. In ECCV. Springer, 2024.
- [50] Zhen Xing, Qi Dai, Zihao Zhang, Hui Zhang, Han Hu, Zuxuan Wu, and Yu-Gang Jiang. Vidiff: Translating videos via multi-modal instructions with diffusion models. arXiv preprint arXiv:2311.18837, 2023.

- [51] Zhen Xing, Qi Dai, Han Hu, Zuxuan Wu, and Yu-Gang Jiang. Simda: Simple diffusion adapter for efficient video generation. In CVPR, 2024.
- [52] Zhen Xing, Qi Dai, Zejia Weng, Zuxuan Wu, and Yu-Gang Jiang. Aid: Adapting image2video diffusion models for instruction-guided video prediction. arXiv preprint arXiv:2406.06465, 2024.
- [53] Zhen Xing, Qijun Feng, Haoran Chen, Qi Dai, Han Hu, Hang Xu, Zuxuan Wu, and Yu-Gang Jiang. A survey on video diffusion models. ACM Computing Surveys, 2024.
- [54] Shiyuan Yang, Liang Hou, Haibin Huang, Chongyang Ma, Pengfei Wan, Di Zhang, Xiaodong Chen, and Jing Liao. Direct-a-video: Customized video generation with user-directed camera movement and object motion. In SIGGRAPH, 2024.
- [55] Zhuoyi Yang, Jiayan Teng, Wendi Zheng, Ming Ding, Shiyu Huang, Jiazheng Xu, Yuanming Yang, Wenyi Hong, Xiaohan Zhang, Guanyu Feng, et al. Cogvideox: Text-to-video diffusion models with an expert transformer. arXiv preprint arXiv:2408.06072, 2024.
- [56] Guy Yariv, Yuval Kirstain, Amit Zohar, Shelly Sheynin, Yaniv Taigman, Yossi Adi, Sagie Benaim, and Adam Polyak. Through-the-mask: Mask-based motion trajectories for image-to-video generation. In CVPR, 2025.
- [57] Shengming Yin, Chenfei Wu, Jian Liang, Jie Shi, Houqiang Li, Gong Ming, and Nan Duan. Dragnuwa: Fine-grained control in video generation by integrating text, image, and trajectory. arXiv preprint arXiv:2308.08089, 2023.
- [58] Tianwei Yin, Michaël Gharbi, Taesung Park, Richard Zhang, Eli Shechtman, Fredo Durand, and William T Freeman. Improved distribution matching distillation for fast image synthesis. In NeurIPS, 2024.
- [59] Tianwei Yin, Michaël Gharbi, Richard Zhang, Eli Shechtman, Frédo Durand, William T Freeman, and Taesung Park. One-step diffusion with distribution matching distillation. In CVPR, 2024.
- [60] Tianwei Yin, Qiang Zhang, Richard Zhang, William T Freeman, Fredo Durand, Eli Shechtman, and Xun Huang. From slow bidirectional to fast autoregressive video diffusion models. In CVPR, 2025.
- [61] Lvmin Zhang, Anyi Rao, and Maneesh Agrawala. Adding conditional control to text-to-image diffusion models. In ICCV, 2023.
- [62] Zhenghao Zhang, Junchao Liao, Menghao Li, Zuozhuo Dai, Bingxue Qiu, Siyu Zhu, Long Qin, and Weizhi Wang. Tora: Trajectory-oriented diffusion transformer for video generation. In CVPR, 2025.
- [63] Zhenghao Zhang, Junchao Liao, Xiangyu Meng, Long Qin, and Weizhi Wang. Tora2: Motion and appearance customized diffusion transformer for multi-entity video generation. arXiv preprint arXiv:2507.05963, 2025.
- [64] Zangwei Zheng, Xiangyu Peng, Tianji Yang, Chenhui Shen, Shenggui Li, Hongxin Liu, Yukun Zhou, Tianyi Li, and Yang You. Open-sora: Democratizing efficient video production for all. arXiv preprint arXiv:2412.20404, 2024.
- [65] Haitao Zhou, Chuang Wang, Rui Nie, Jinlin Liu, Dongdong Yu, Qian Yu, and Changhu Wang. Trackgo: A flexible and efficient method for controllable video generation. In AAAI, 2025.

Appendix

6 Additional Ablation results

6.1 Quantitative Results

Here, we provide the complete quantitative results across all three benchmarks, including FlashBench, MagicBench [18], and DAVIS [28] in Table. 4 and Table. 5. All ablation studies are trained for 1K steps on 4 Nvidia A100 GPUs, with other training configurations kept consistent with FlashMotion Stage 3.

Table 4 Comprehensive ablation study of FlashMotion. We analyze both adapter variants (ResNet and ControlNet) by progressively removing key components — including the *FastAdapter* training stage, diffusion loss, GAN loss, and the dynamic diffusion loss scaling strategy. The results show that each component plays a crucial role in preserving high video quality and precise motion alignment.

Methods	FlashBench			MagicBench			DAVIS		
	FID(↓)	FVD(↓)	M/B IoU%(↑)	FID(↓)	FVD(↓)	M/B IoU%(↑)	FID(↓)	FVD(↓)	M/B IoU%(↑)
Adapter Type: ResNet									
Slow Adapter	22.75	168.46	49.79 / 56.62	21.59	162.93	60.24 / 67.23	52.01	992.26	36.33 / 51.37
w/o Diffusion Loss	18.87	161.07	52.04 / 58.04	21.95	162.31	63.14 / 69.02	55.28	983.91	37.22 / 52.47
w/o GAN Loss	22.74	206.75	65.82 / 70.60	30.51	167.91	73.86 / 78.48	66.46	1015.81	47.13 / 62.58
w/o Dynamic Scale	26.32	210.93	65.54 / 69.77	21.90	167.00	73.60 / 78.15	73.12	998.85	47.01 / 60.12
FlashMotion	15.81	108.96	63.96 / 70.01	14.16	109.20	72.34 / 77.92	50.58	786.42	46.74 / 64.00
Adapter Type: ControlNet									
Slow Adapter	19.44	171.83	62.72 / 69.38	21.19	161.80	70.20 / 76.54	46.42	875.37	50.52 / 70.83
w/o Diffusion Loss	21.21	172.04	55.91 / 61.59	22.36	176.01	66.25 / 71.82	49.27	882.81	42.46 / 59.01
w/o GAN Loss	28.82	265.46	71.56 / 75.48	26.33	192.85	78.26 / 82.15	75.42	1131.65	55.87 / 68.59
w/o Dynamic Scale	19.93	155.55	70.46 / 75.89	16.83	131.59	77.49 / 82.29	61.47	958.22	55.51 / 70.13
FlashMotion	14.35	96.08	69.15 / 75.38	12.49	99.30	76.92 / 82.17	45.66	690.13	54.54 / 74.37

Table 5 Ablation study on the discriminator architecture. VC denotes the *Video Cross-Attention* layer, SS denotes the *Semantic Self-Attention* layer, and TC denotes the *Trajectory Cross-Attention* layer. Results show that our discriminator design achieves the best overall performance across all benchmarks and metrics.

Methods	FlashBench			MagicBench			DAVIS		
	FID(↓)	FVD(↓)	M/B IoU%(↑)	FID(↓)	FVD(↓)	M/B IoU%(↑)	FID(↓)	FVD(↓)	M/B IoU%(↑)
Adapter Type: ResNet									
VC only	16.76	110.83	62.07 / 67.76	14.73	114.61	71.00 / 75.86	53.22	800.50	43.97 / 60.16
SS+VC	16.31	109.02	62.54 / 68.05	14.44	113.88	71.16 / 76.28	52.34	830.14	44.61 / 62.50
TC+VC	16.64	110.01	62.99 / 69.36	14.87	114.11	71.70 / 77.31	53.16	830.57	45.11 / 62.56
FlashMotion	15.81	108.96	63.96 / 70.01	14.16	109.20	72.34 / 77.92	50.58	786.42	46.74 / 64.00
Adapter Type: ControlNet									
VC only	15.56	115.72	63.04 / 71.73	13.71	120.22	75.78 / 81.33	49.39	798.79	51.48 / 69.00
SS+VC	15.37	99.24	65.84 / 72.35	13.42	101.58	75.35 / 81.06	46.24	711.82	53.33 / 71.99
TC+VC	15.70	101.06	68.78 / 73.85	13.96	105.49	76.48 / 82.15	48.50	758.96	53.91 / 72.90
FlashMotion	14.35	96.08	69.15 / 75.38	12.49	99.30	76.92 / 82.17	45.66	690.13	54.54 / 74.37

Fast Adapter To assess the importance of the *FastAdapter* training stage, we evaluate the performance of directly applying *SlowAdapter* to *FastGenerator* across all three benchmarks. As shown in Table 4, removing

the *FastAdapter* stage results in a consistent decline in both video quality and trajectory accuracy across all benchmarks, underscoring the necessity of the additional *FastAdapter* training stage.

Diffusion Loss To evaluate the role of the diffusion loss, we remove it during training and measure performance across all benchmarks. As presented in Table 4, removing the diffusion loss leads to a noticeable drop in trajectory alignment for both adapter architectures. This shows that the diffusion loss is essential for maintaining trajectory consistency between generated motions and user-specified trajectories. Moreover, its removal also causes a degradation in both image and video quality.

GAN Loss We conduct an ablation study on the GAN loss, as summarized in Table 4. While removing the adversarial objectives slightly improves trajectory accuracy, it causes an approximately 90% reduction in both image and video quality, introducing severe blurring artifacts.

Dynamic Diffusion Loss Scaling We further validate the effectiveness of the proposed dynamic diffusion loss scaling strategy by fixing the loss scale to 1 during training. As shown in Table 4, disabling dynamic scaling leads to a clear decline in both image and video quality across all three benchmarks, again resulting in noticeable blurring artifacts.

Discriminator Architecture Finally, we assess the impact of different discriminator architectures, as shown in Table 5. Using only the *Video Cross-Attention* layer yields the lowest performance in both visual quality and trajectory accuracy. In contrast, incorporating the *Semantic Self-Attention* module enhances the model’s semantic understanding, improving visual realism, while the *Trajectory Cross-Attention* module strengthens trajectory control accuracy. Overall, our full discriminator architecture achieves the best results across all evaluation metrics and benchmarks.

6.2 More Qualitative Results

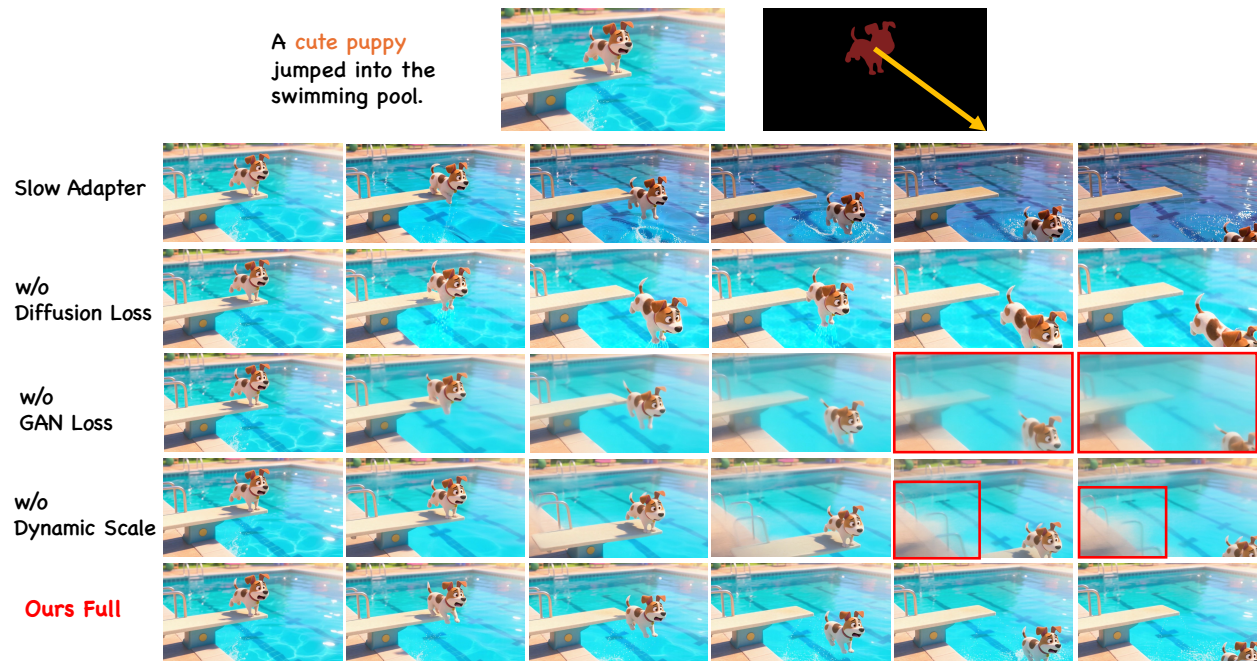


Figure 6 Additional ablation study results. Only our full method can generate videos with both high visual quality and trajectory accuracy.



Figure 7 Additional ablation study results. Only our full method can generate videos with both high visual quality and trajectory accuracy.

Detailed qualitative ablation results are presented in Fig.6, Fig.7, and Fig.8. As shown, directly applying *SlowAdapter* to *FastGenerator* produces pronounced artifacts—such as the color drift in Fig.6 and Fig.8, and the distorted object shapes in Fig.7. In addition, removing the diffusion loss during training markedly degrades trajectory fidelity: objects (e.g., the dog or the bus) drift away from the intended paths, and in the extreme case shown in Fig. 8, a single Spongebob is mistakenly duplicated into two. Finally, eliminating either the GAN loss or the dynamic scale strategy introduces severe blurring artifacts.

7 Additional Comparison results

7.1 Backbone Comparisons

As shown in Table 6, we present a comprehensive comparison of the backbone architectures used across different methods. The table summarizes the supported video length and spatial resolution, as well as the corresponding denoising latency and total parameter count. Notably, FlashMotion achieves the fastest denoising speed for both the ControlNet- and ResNet-based adapters, while also supporting the highest resolution and the longest generation length. Depending on their needs, users can flexibly choose between the ResNet or ControlNet variants of FlashMotion to balance generation speed, video quality, and trajectory accuracy.

7.2 Results Across Object Counts

Due to space limitations, the main paper only reports the overall quantitative comparison on FlashBench. Here, we present detailed evaluations under different numbers of controlled objects, covering cases from 1–5 to more than 5 foreground objects. As shown in Table 7 and Table 8, the ControlNet variant of FlashMotion consistently surpasses all competing methods across all metrics, outperforming both multi-step and few-step baselines in terms of visual quality and trajectory accuracy. When using a ResNet-based trajectory adapter, FlashMotion also achieves better visual quality than the previous SOTA method MagicMotion [18], though it still falls slightly short in trajectory accuracy due to the limited parameter capacity.

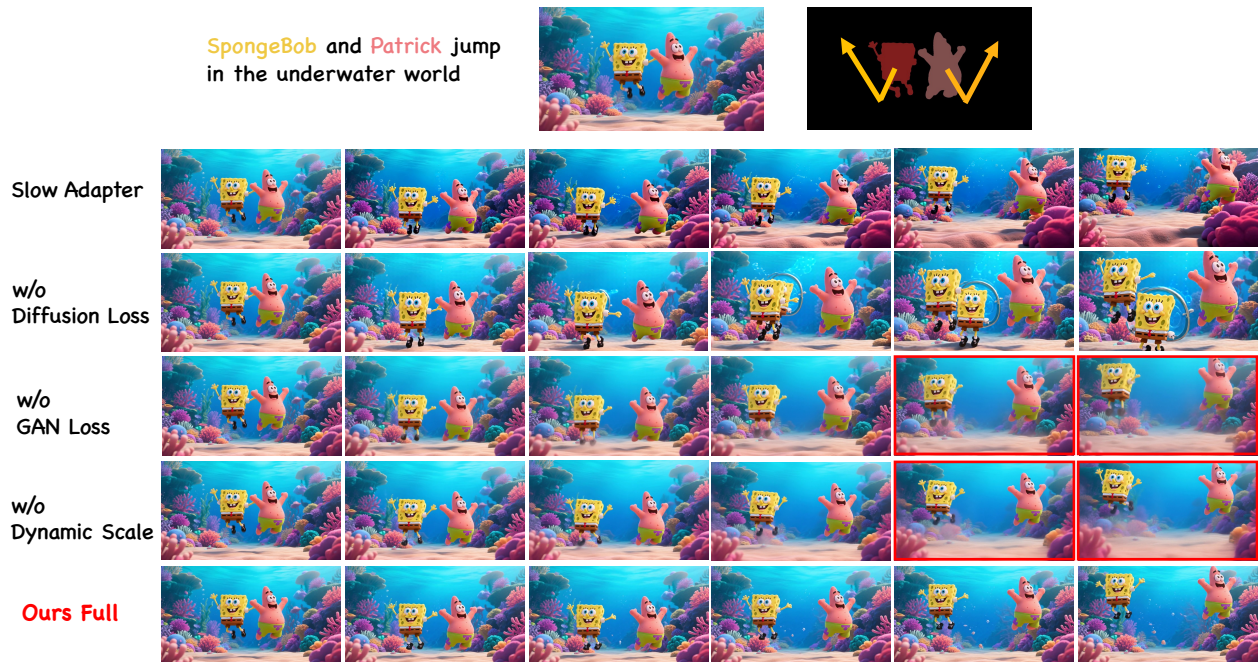


Figure 8 Additional ablation study results. Only our full method can generate videos with both high visual quality and trajectory accuracy.

7.3 More Qualitative Results

In this section, we present additional qualitative comparisons with previous methods. As illustrated in Figs. 9–15, FlashMotion accurately controls object trajectories and produces high-quality videos, whereas the other approaches exhibit notable artifacts and inconsistencies. For full video results, please refer to “Supplementary video.mp4” in the supplementary material.

8 Case Studies

8.1 Different Styles

As shown in Fig. 16, FlashMotion supports generating videos across diverse visual styles, including dreamlike realism, surreal miniature photography, 3D cartoon rendering, and Eastern ink-wash painting. To better demonstrate the model’s robustness and its ability to maintain consistent motion across challenging layouts, we deliberately choose vertically oriented images instead of horizontal ones. These examples collectively illustrate FlashMotion’s strong adaptability to various artistic domains while preserving coherent structure and motion.

8.2 Camera Control

FlashMotion supports camera control operations such as zooming in and zooming out. As shown in Fig.17, the camera motion can be adjusted by manipulating the bounding box size of the foreground object, such as the cup or the woman’s mask. Furthermore, as illustrated in Fig.18, users can navigate scenes—like a bakery or a museum—by controlling the bounding boxes of objects such as the dinosaur, the mammoth, or the industrial mixer.

Table 6 Comparison of model configurations and backbone architectures, including supported video length, spatial resolution, denoising latency, and total parameters. FlashMotion achieves the fastest denoising speed while supporting the highest resolution and longest generation length.

Method	Video Length	Video Resolution	Denoising Latency(s)	Total Params(B)	Base Model
LeviTor [41]	16	288×512	80.08	2.21	SVD [1]
DragAnything [49]	14	320×576	589.07	2.21	SVD [1]
SG-I2V [26]	14	576×1024	1277.15	1.52	SVD [1]
Tora [62]	49	480×720	691.13	6.32	CogVideoX [55]
MagicMotion [18]	49	480×720	1158.63	11.53	CogVideoX [55]
Wan+ResNet [40]	121	704×1280	333.00	5.02	Wan2.2 [40]
Wan+ControlNet [40]	121	704×1280	664.53	10.28	Wan2.2 [40]
FlashMotion (ResNet)	121	704×1280	11.72	5.02	Wan2.2 [40]
FlashMotion (ControlNet)	121	704×1280	24.44	10.28	Wan2.2 [40]

Table 7 Quantitative comparison results on FlashBench for scenes containing 1, 2, and 3 controlled objects. The detailed evaluations show that FlashMotion with a ControlNet-based adapter consistently outperforms all competing methods across all metrics, while the ResNet-based adapter also delivers superior visual quality compared to prior work.

Methods	Obj_Num=1			Obj_Num=2			Obj_Num=3		
	FID(↓)	FVD(↓)	M/B IoU(↑)	FID(↓)	FVD(↓)	M/B IoU(↑)	FID(↓)	FVD(↓)	M/B IoU(↑)
MultiSteps (50 Steps)									
MagicMotion [18]	53.62	741.91	67.93/83.46	59.37	697.50	61.05/73.47	52.44	563.38	66.13/72.92
Wan2.2 (ResNet) [40]	49.01	599.93	61.10/76.34	56.19	582.42	51.49/62.07	57.39	566.53	50.06/56.75
Wan2.2 (ControlNet) [40]	50.04	594.54	66.07/83.98	<u>51.20</u>	591.56	59.64/73.18	49.49	547.90	62.64/70.01
DragAnything [49]	76.28	1076.20	62.70/74.88	91.08	1196.46	53.34/63.06	89.26	1099.45	54.01/57.55
SG-I2V [26]	70.20	984.94	64.09/76.45	78.93	926.79	47.16/57.04	73.08	891.52	48.31/54.25
Tora [62]	73.15	902.55	58.24/69.00	80.27	939.72	46.45/57.47	82.54	869.43	46.80/52.66
LeviTor [41]	128.25	1318.56	49.63/59.73	127.24	1124.07	38.09/44.82	131.60	1252.00	35.65/39.08
FewSteps (4 Steps) — Adapter: ResNet									
DMD [58]	64.71	709.74	55.34/74.30	63.28	687.09	45.21/59.62	64.03	636.34	43.08/53.14
GAN [6]	79.73	728.35	54.58/66.52	77.25	700.88	41.38/51.34	74.52	673.58	41.46/48.80
LCM [22]	58.97	875.26	64.61/80.06	72.26	1032.56	56.40/68.58	65.52	1033.12	53.52/59.67
FlashMotion	<u>46.64</u>	<u>509.36</u>	<u>68.02/84.86</u>	51.21	<u>497.62</u>	60.27/73.08	<u>44.41</u>	<u>433.60</u>	63.40/71.59
FewSteps (4 Steps) — Adapter: ControlNet									
DMD [58] / GAN [6]	OOM								
LCM [22]	61.13	851.48	62.83/76.15	76.41	929.77	56.68/66.79	69.65	831.79	57.86/63.51
FlashMotion	44.97	465.86	68.44/84.51	46.16	437.18	63.87/76.99	42.20	422.16	66.45/73.91

9 More Details on FlashBench

FlashBench comprises 600 videos, grouped into six categories based on the number of foreground objects (ranging from 1–5 and more than 5). To offer a more comprehensive analysis of the dataset, we further visualize the distributions of video lengths as shown in Fig. 19, demonstrating its support for evaluating long video generation.

Table 8 Quantitative comparison results on FlashBench for scenes containing 4, 5, and above 5 controlled objects. The detailed evaluations show that FlashMotion with a ControlNet-based adapter consistently outperforms all competing methods across all metrics, while the ResNet-based adapter also delivers superior visual quality compared to prior work.

Methods	Obj_Num=4			Obj_Num=5			Obj_Num>5		
	FID(↓)	FVD(↓)	M/B IoU(↑)	FID(↓)	FVD(↓)	M/B IoU(↑)	FID(↓)	FVD(↓)	M/B IoU(↑)
MultiSteps (50 Steps)									
MagicMotion [18]	45.67	546.40	<u>70.29/73.21</u>	44.41	450.10	<u>73.86/76.93</u>	44.41	409.25	<u>69.29/62.35</u>
Wan2.2 (ResNet) [40]	61.69	575.65	50.89/53.93	52.04	476.04	55.56/56.98	41.59	453.60	44.31/41.03
Wan2.2 (ControlNet) [40]	49.25	503.03	66.15/68.65	43.58	409.57	70.70/70.94	37.11	406.06	67.27/61.05
DragAnything [49]	75.00	997.03	59.97/60.23	83.35	812.67	62.92/61.48	97.48	1006.25	56.95/49.51
SG-I2V [26]	64.83	861.49	50.87/55.46	65.91	713.41	54.21/55.83	66.22	828.14	36.75/35.52
Tora [62]	65.25	737.03	46.28/51.05	73.88	714.65	52.76/54.55	93.60	1073.05	37.98/36.89
LeviTor [41]	167.97	1774.66	35.10/34.02	185.75	2015.57	33.33/30.34	135.75	1287.67	24.23/23.41
FewSteps (4 Steps) — Adapter: ResNet									
DMD [58]	66.08	749.99	41.38/48.44	67.03	697.32	42.02/47.94	52.62	671.65	32.74/32.74
GAN [6]	69.55	571.76	45.87/50.43	65.83	500.22	48.67/52.49	59.83	584.86	31.00/30.78
LCM [22]	62.24	959.97	57.30/57.89	58.71	869.45	56.78/58.98	49.66	780.45	43.51/40.21
FlashMotion	<u>38.47</u>	<u>411.71</u>	66.58/67.87	<u>39.53</u>	<u>326.98</u>	68.67/79.78	<u>37.07</u>	<u>384.06</u>	56.92/52.02
FewSteps (4 Steps) — Adapter: ControlNet									
DMD [58] / GAN [6]	OOM								
LCM [22]	60.28	752.48	63.18/63.38	56.29	637.06	66.48/65.66	53.64	541.55	60.79/53.62
FlashMotion	36.62	367.24	71.81/75.49	35.19	294.47	74.94/76.98	32.72	305.68	69.43/64.50

A tiny hamster in a pistachio hat drives a bread-bulldozer, pushing rainbow sprinkles across the floor.

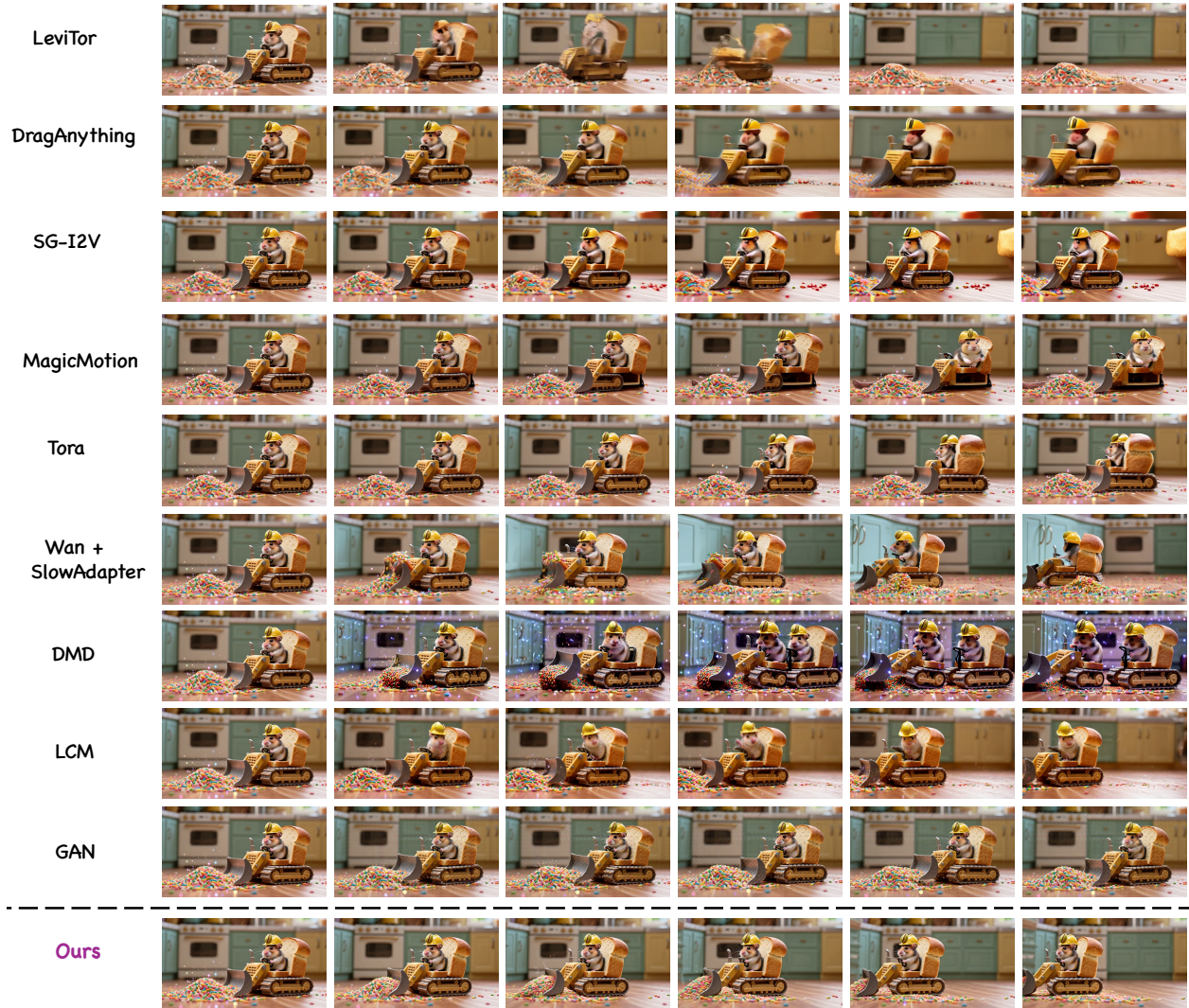


Figure 9 Qualitative Comparisons results with different methods.

Mars moves in the sky and the Earth gradually sinks into the sea.

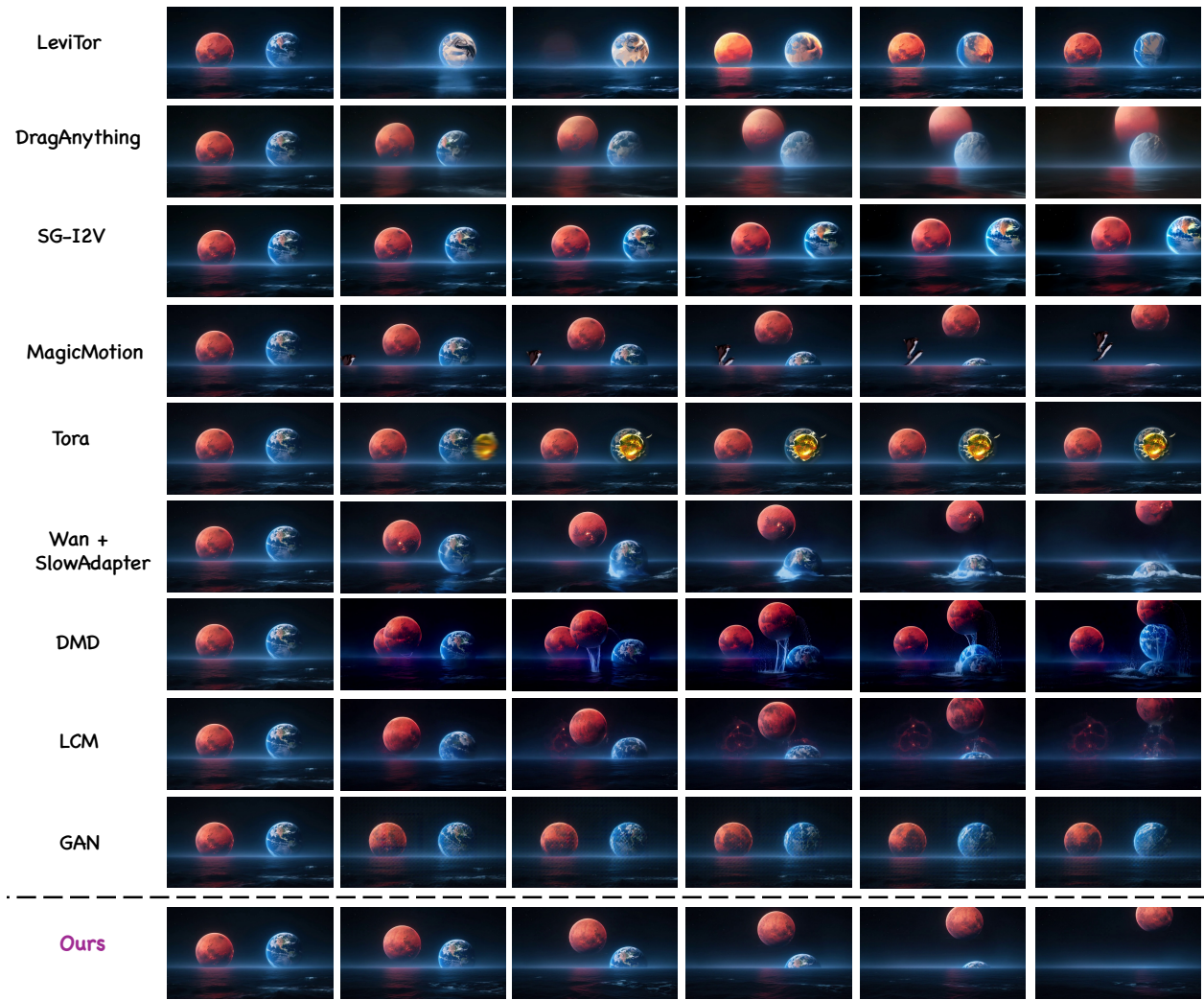


Figure 10 Qualitative Comparisons results with different methods.

A cowboy riding a horse in the wilderness

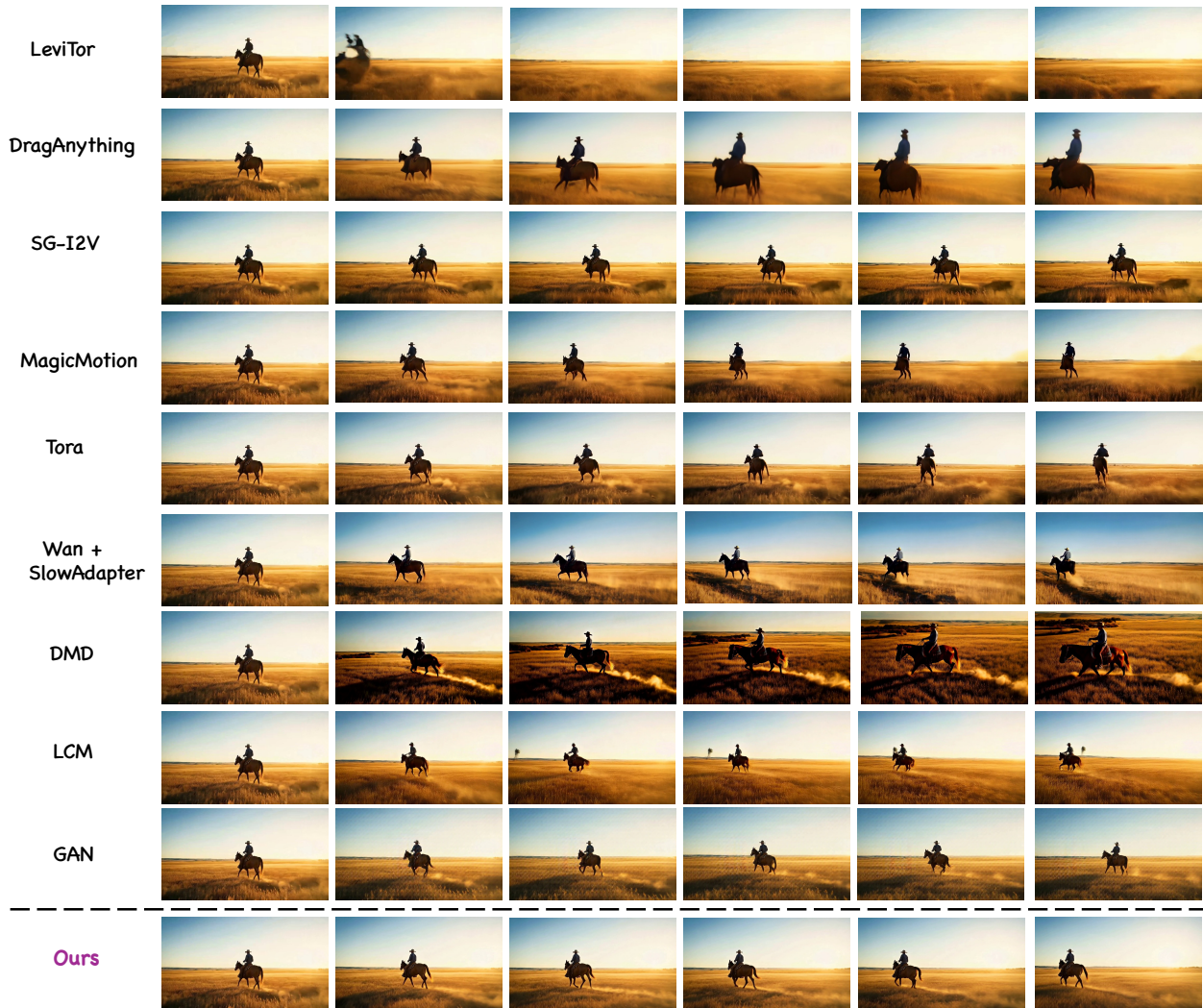
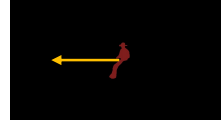


Figure 11 Qualitative Comparisons results with different methods.

An astronaut walking towards a spaceship

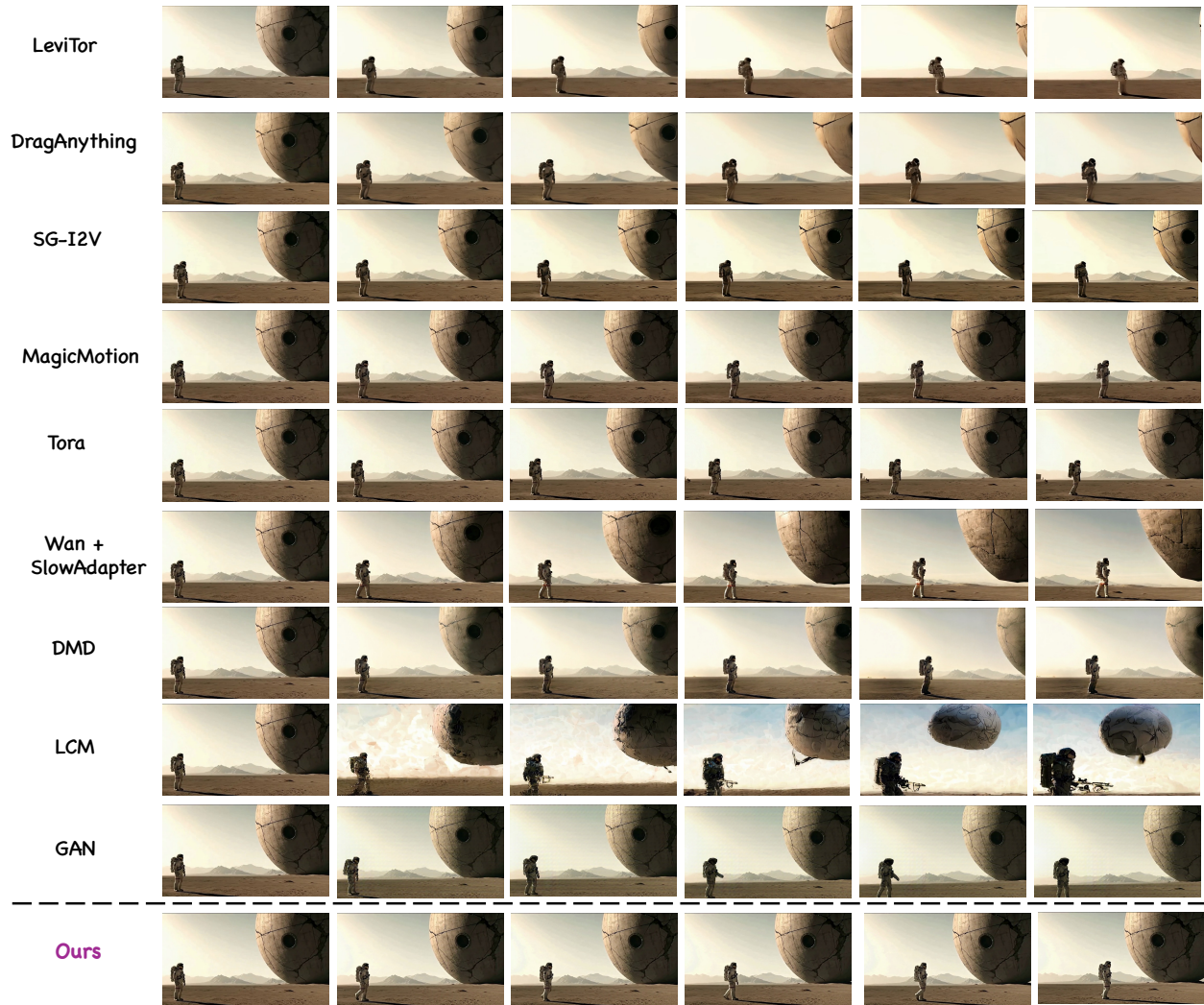


Figure 12 Qualitative Comparisons results with different methods.

A soldier with a lightning bolt emblazoned on his chest runs on the battlefield

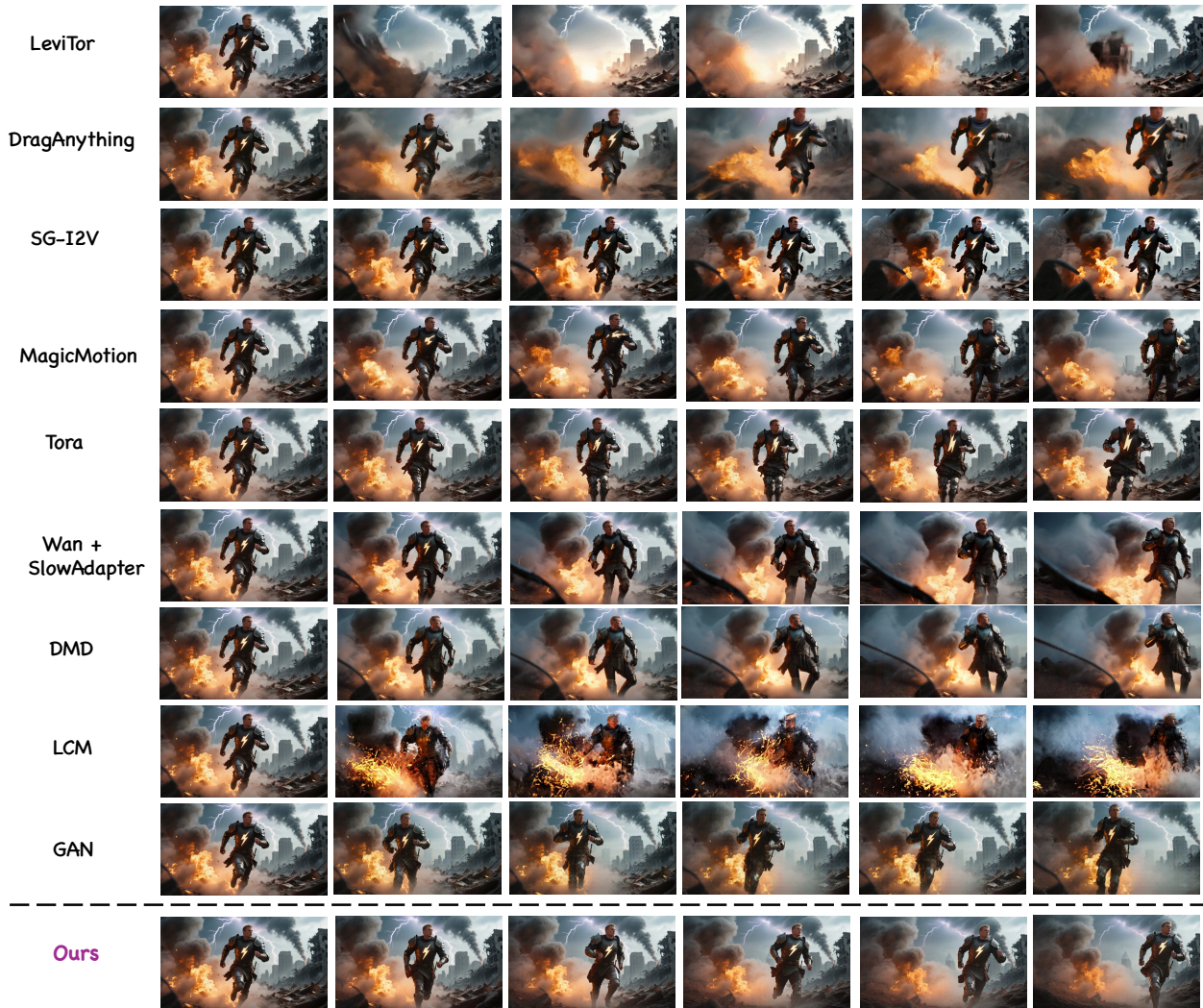


Figure 13 Qualitative Comparisons results with different methods.

A Chinese god shakes the
luminous pearl in his hand

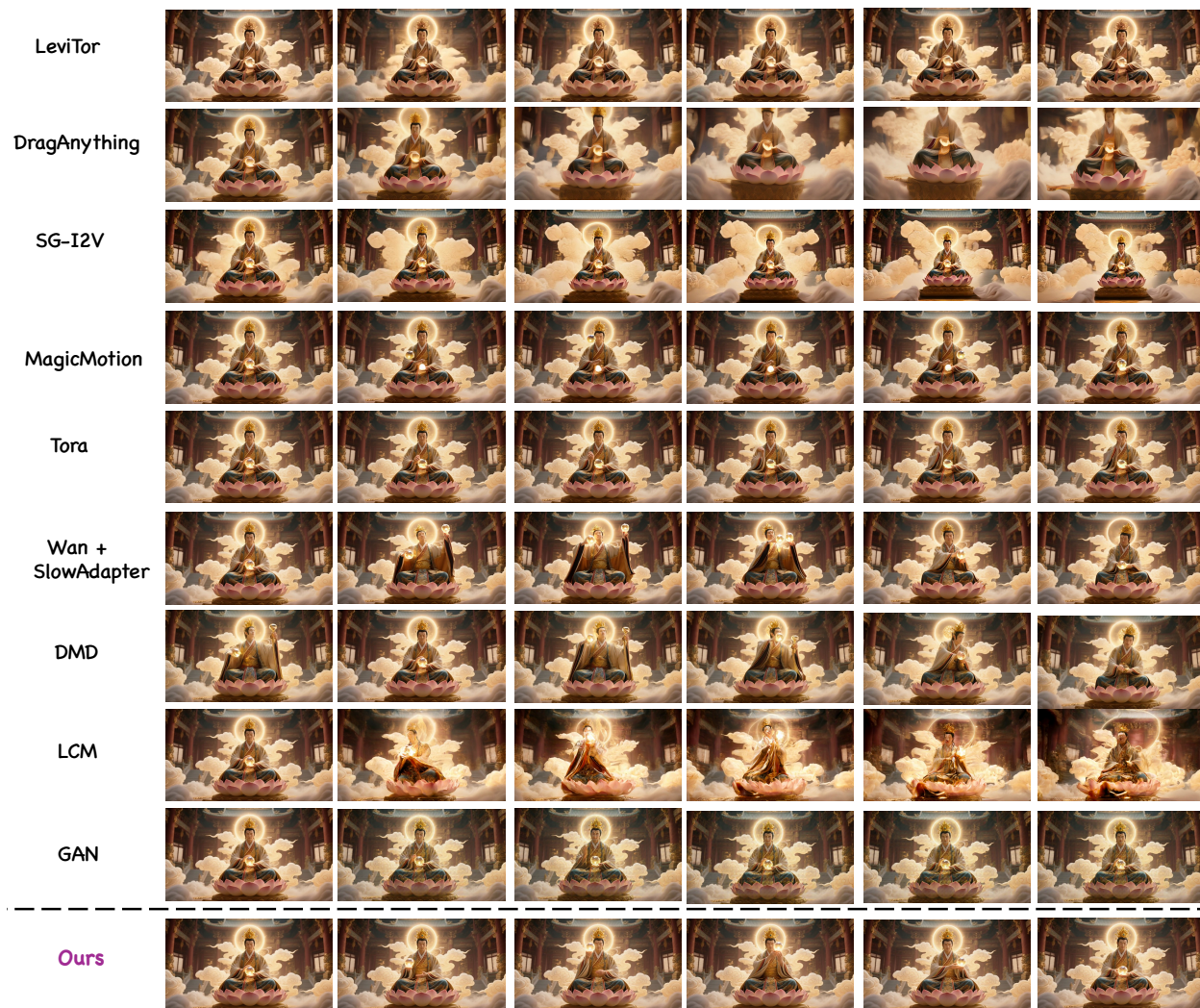


Figure 14 Qualitative Comparisons results with different methods.

Doctor Strange wiggles his fingers and casts a spell

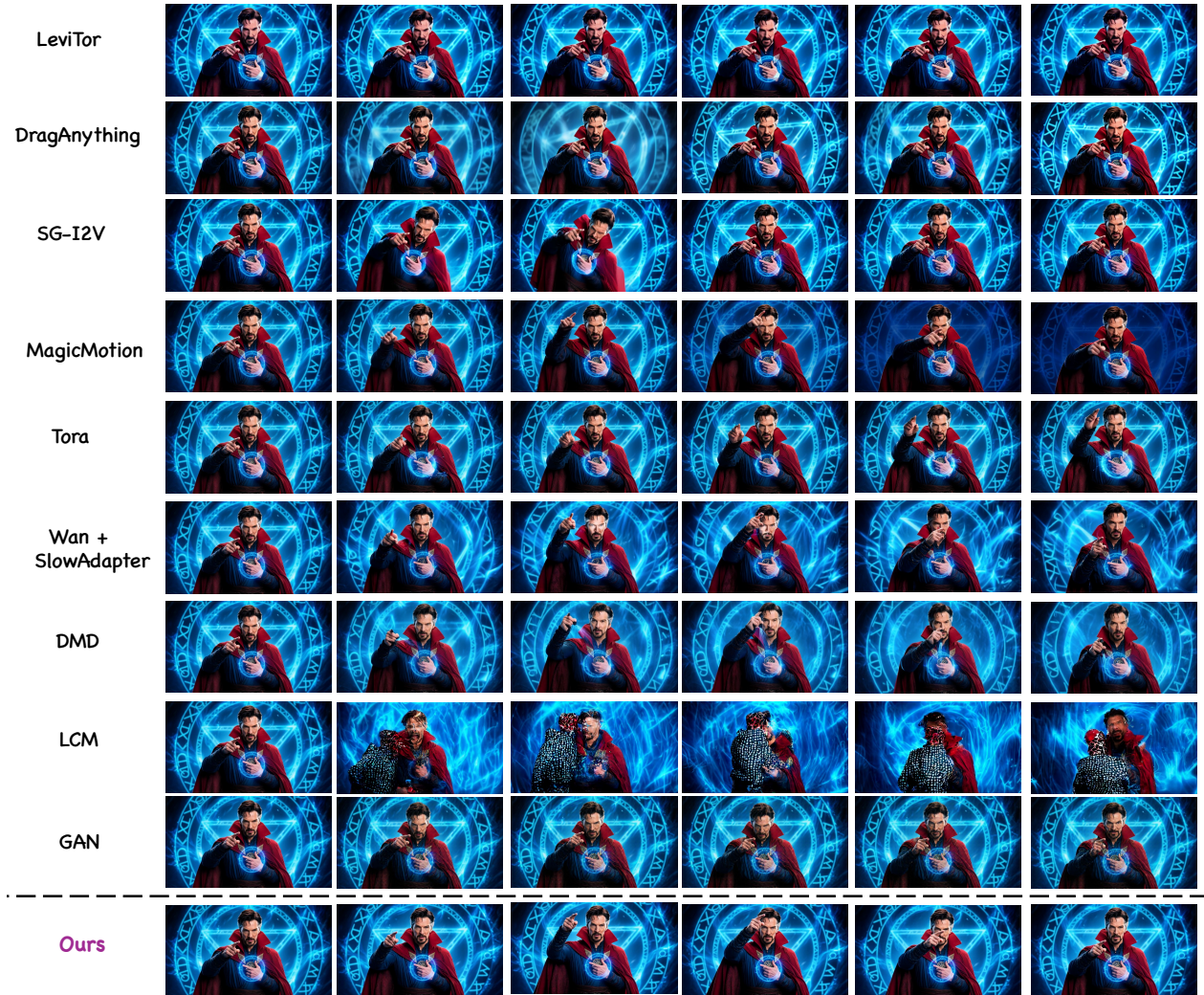


Figure 15 Qualitative Comparisons results with different methods.

**Dreamlike
Realism**



**Surreal
Photography**



Cartoon



Ink Painting



Figure 16 FlashMotion supports generating videos of different styles.

Zoom In



Zoom Out



Figure 17 FlashMotion enables controllable camera movements, such as zooming in or out, by adjusting the bounding box size of the foreground object (e.g., the cup or the woman's mask).

Museum



Bakery



Figure 18 FlashMotion supports scene navigation in various environments—such as a bakery or a museum—by manipulating the bounding boxes of key objects, including the dinosaur, the mammoth, and the industrial mixer.

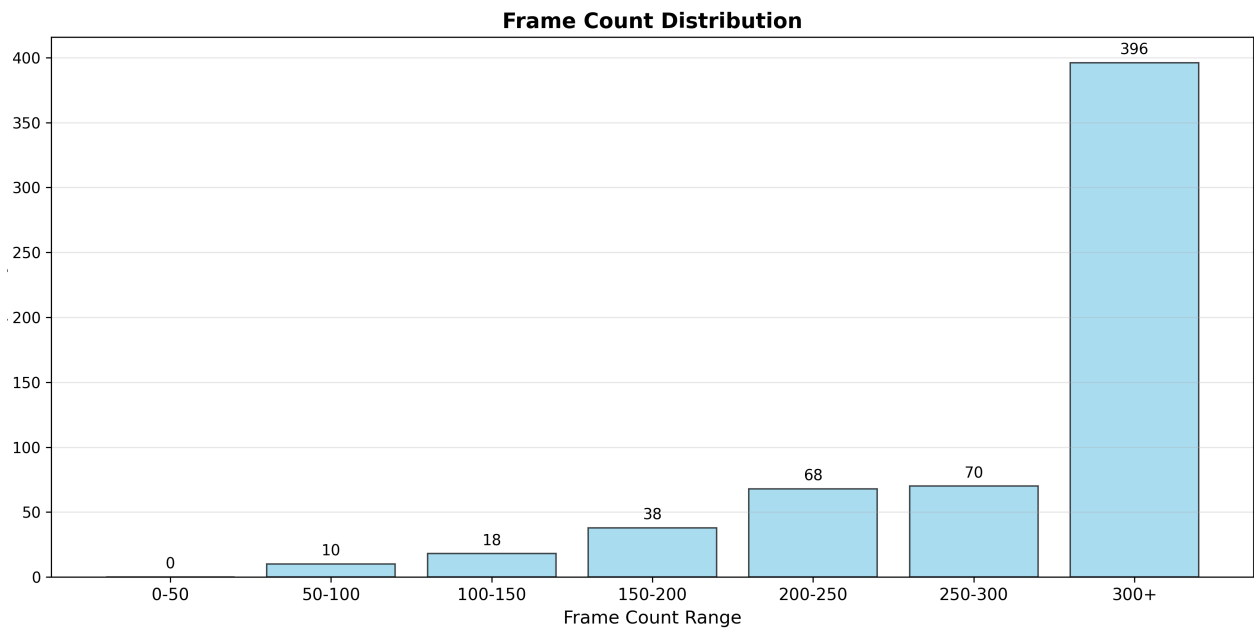


Figure 19 Distribution of video frame counts in FlashBench, demonstrating its support for evaluating long video generation.